Journal of Petroleum Geology

www.jpg.co.uk

Journal of Petroleum Geology, Vol. 43(1), January 2020, pp 27-48


# GAS-HYDRATE SYSTEMS AND GAS VOLUMETRIC ASSESSMENT IN THE LOWER FANGLIAO BASIN, TAIWAN ACCRETIONARY WEDGE

**F. Dirgantara [1,2], A.T-S. Lin[1,2*], C-S. Liu[3], C-C. Lin[2] and S-C. Chen[4]**

*The accretionary wedge in the incipient arc-continent collisional zone offshore southwestern Taiwan is rich in gas hydrates as inferred from reflection seismic data and the geochemical analyses of shallow sediments. In this study, 2D and 3D seismic data were used to investigate the role of structural factors including mud diapirism on the formation of gas hydrates and associated free gas in the Quaternary Lower Fangliao Basin, a semi-enclosed slope basin situated on the upper accretionary wedge. Albeit limited drilling information on lithostratigraphy and petroleum potential in the area together with seismic reflection data show that mud diapirs have influenced the formation of bottom-simulating reflectors (BSRs) and the distribution of gas hydrates and free gas. On reflection seismic profiles, five seismic facies were observed and are characterised by: stratified parallel reflections; contorted reflections; semi-parallel, high-amplitude reflections; oblique, continuous high-amplitude reflections; and generally transparent reflections. These seismic facies were respectively interpreted as hemipelagic sediments, mass transport deposits (MTDs), sandstone-rich turbidites, overbank deposits and mud diapirs. The gas hydrate stability zone (GHSZ) is characterized by (i) high amplitude reflections with an analogous phase to that of seafloor, possibly indicating potential porous sandstone-rich turbidite reservoirs; (ii) BSRs showing polarity reversal relative to seafloor, suggesting higher impedance gas hydrates overlying lower impedance intervals with free gas; (iii) blanking reflections in fault zones, interpreted as gas-bearing fluid conduits; (iv) strong reflections on the flanks of mud diapirs (e.g. flank drags) and above buried mud diapirs, demonstrating the presence of gas hydrates; (v) high amplitude reflections dragging on diapiric flanks with reversed phase to that of seafloor, indicating free gas -charged zones abutting mud diapirs; and (vi) the presence of focused advection and diffusion flow through mud diapirs and faults, which is interpreted to control the migration of thermogenic gas. Based on the distribution of seismic amplitude characteristics and reflection strength with respect to depth of the BSRs, hydrocarbon prospects can be divided into gas-hydrate compartments above BSRs, free gas compartments above BSRs, and free gas compartments below BSRs. From a combination of geobody extraction and Monte Carlo simulation, the prospects appear to hold about 2048 Bcf (billion cubic feet) of total gas volume over a study area of 60 km$^2$. These observations provide first-order estimates of methane resources in the Lower Fangliao Basin offshore southwestern Taiwan.*

[1] Earth System Science Program, Taiwan International Graduate Program, Academia Sinica and National Central University, Taiwan.
[2] Department of Earth Sciences, National Central University, No. 300, Zhongda Rd, Zhongli District, Taoyuan, 32001, Taiwan.

*corresponding author, andrewl@ncu.edu.tw

**Key words**: gas hydrates, free gas, BSRs, seismic facies, volumetric estimation, mud diapirism, accretionary wedge, Lower Fangliao Basin, Taiwan.

[3] Ocean Center, National Taiwan University, No. 1, Sec. 4, Roosevelt Rd, Taipei 10617, Taiwan.
[4] Central Geological Survey, Ministry of Economic Affairs, No. 2, Ln. 109, Huaxin St, Zhonghe Dist., New Taipei City, 235, Taiwan.

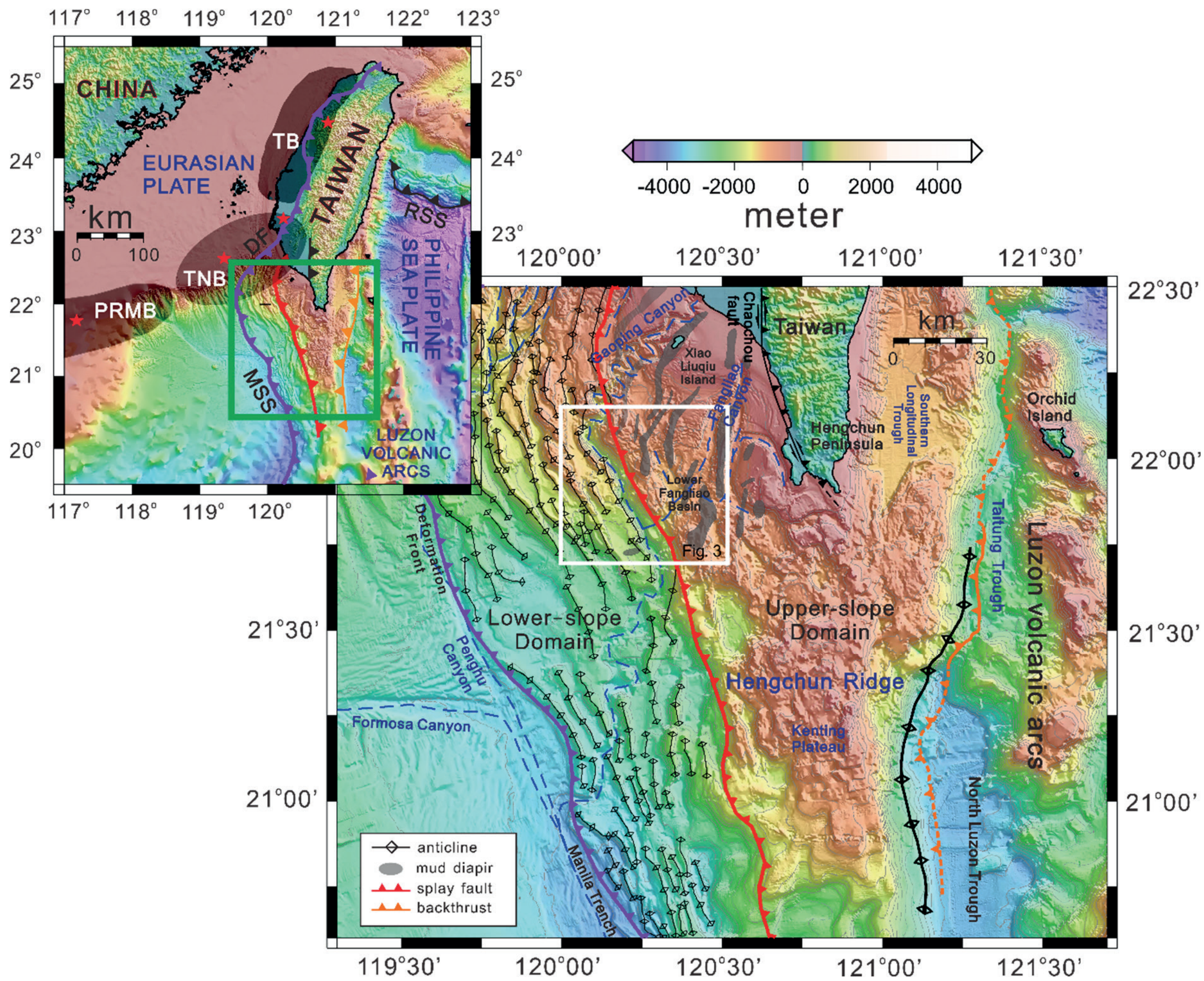


**Fig. 1. (above, left) Regional map of Taiwan and the surrounding area showing major tectonic elements. Abbreviations: TB: Taihshi Basin; TNB: Tainan Basin; PRMB: Pearl River Mouth Basin; RSS: Ryukyu Subduction System; MSS: Manila Subduction System; DF: Deformation Front. The green square shows the location of the bathymetric map (at right) of southern Taiwan and the adjacent offshore areas; the white square shows the study area depicted in Fig. 3. The Lower Fangliao Basin is located in the upper slope domain of the Taiwan accretionary wedge. Offshore structures are from Lin *et al.* (2008, 2009a). On- and offshore hydrocarbon fields are marked by red stars (from Lee *et al.*, 1993; Zhou and Yao, 2009).**

## INTRODUCTION

Gas-hydrate systems associated with submarine mud diapirism have been reported in a number of deep-water settings (Westbrook and Smith, 1983; Milkov, 2000, Hsu *et al.*, 2017). Submarine mud diapirism typically occurs at convergent plate boundaries, for example in the inner and outer Sunda Arc (Satyana and Asnidar, 2009), offshore Eastern Timor (Barber *et al.*, 1986), offshore Barbados (Westbrook and Smith, 1983) and in the Nankai Trough (Moore *et al.*, 2001). Mud diapirism is in general confined to areas with rapid sedimentation rates and vertical sediment loading; the generation and accumulation of hydrocarbons may lead to overpressuring and fluid expulsion due to clay mineral dehydration (Tissot and Welte, 1984).

In convergent margins, water-rich and organic-rich marine sediments may be affected by compressive stresses as they are incorporated into accretionary wedges which may be imbricated and deformed in compressional fold-and-thrust belts. Submarine mud volcanoes and diapirs form as a consequence of fluid migration along diapiric bodies, and gas migration from deep-marine sediments into near-surface sediments or seawater may also occur (Milkov, 2000). Hydrocarbons associated with mud diapirism are not exclusively biogenic (Chuang *et al.*, 2010; Chen *et al.*, 2014) but may have thermogenic (Sun *et al.*, 2010) or abiogenic origins (Johnson *et al.*, 2015).

In the northern rifted margin of the South China Sea, gas migration through faults and mud diapirs has contributed to the accumulation of shallow gas hydrates (McDonnell *et al.*, 2000; Liu *et al.*, 2006). In this area, the distribution of gas hydrates is largely associated with gas chimneys and faults which provide pathways for fluid migration into the gas hydrate stability zone (GHSZ) (e.g. Li *et al.*, 2013). Folds and thrusts in the upper slope of the Taiwan accretionary prism (Fig. 1) serve as migration pathways for buoyancy-driven deep-seated fluids (Hsu *et al.*, 2017).

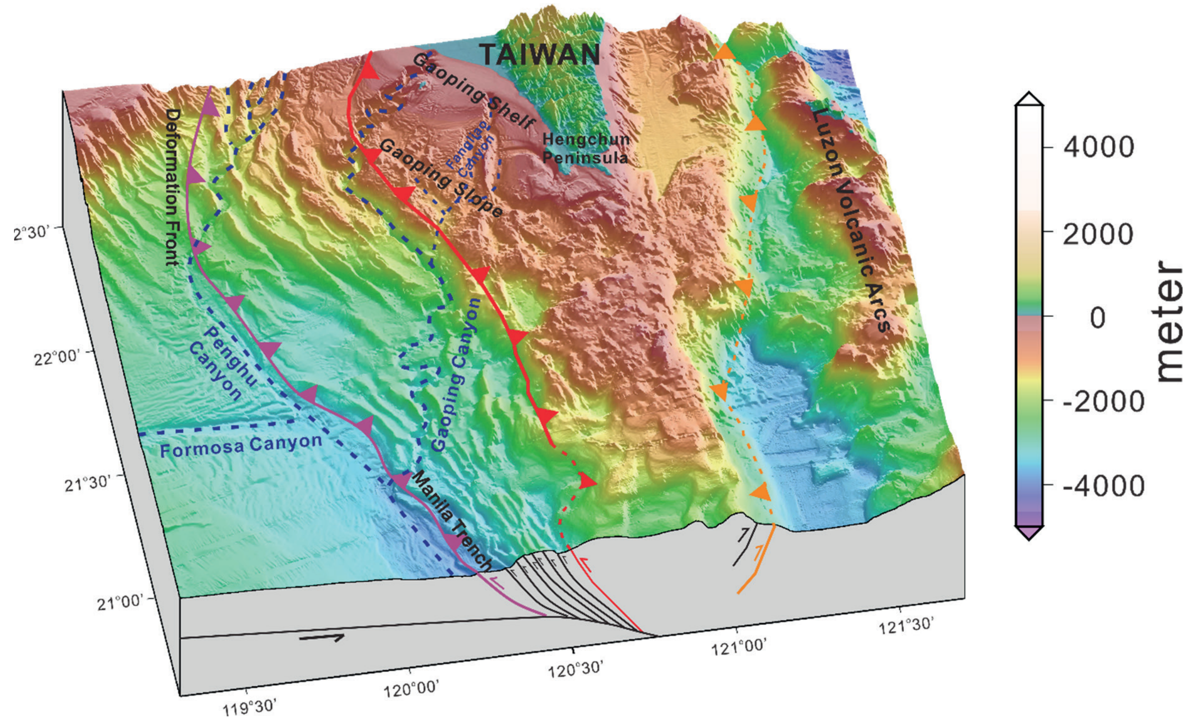


**Fig. 2. Block diagram showing the bathymetry and morphology of offshore SW and southern Taiwan with (below) a simplified structural cross-section. The purple line indicates the deformation front to the north which passes to the south into the Manila Trench, marking the transition from a subduction system into an incipient arc-continent collision zone. The red line highlights the splay fault that separates the upper Gaoping slope from the lower Gaoping slope. The yellow line marks an inferred backthrust. Offshore structures are from Lin *et al.* (2008, 2009a).**

The study area offshore southwestern Taiwan is located in the collision zone between the Luzon Arc of the Philippine Sea Plate and the Eurasian Plate (Fig. 1), and is characterised by the presence of submarine mud diapirs, mud volcanoes and gas seepages (Reed *et al.*, 1992; Chen *et al.*, 2014). Preliminary studies by the Chinese Petroleum Corporation in the early 1970s suggested that the area had little prospectivity (Sun and Liu, 1993). However, extensive geological, geophysical and geochemical studies by the Taiwanese Central Geological Survey since the mid-2000s have shown that significant volumes of gas hydrates and free gas may occur in this area (Chung *et al.*, 2016). The area is characterized by the presence of active compressive structures and a deformation front separating the convergent zone from the South China Sea (SCS) rifted continental margin. In this setting, the pressure and temperature conditions allow the formation of gas hydrates at water depths of 500 to 3000 m (Liu *et al.*, 2006). Bottom-simulating reflectors (BSRs) have been reported from seismic surveys carried out in the area (Chi *et al.*, 1998; Liu *et al.*, 2006; Hsu *et al.*, 2017) and have been complemented by geochemical studies of shallow seabed anomalies related to the presence of gas hydrates and associated free gas (Chen *et al.*, 2017).

This study aims to investigate the influence of mud diapirism on the occurrence of gas hydrates and associated free gas in the Lower Fangliao Basin in the upper accretionary wedge, offshore southwestern Taiwan (Fig. 1). 2D and 3D seismic data were used to study the dynamics of fluid migration and accumulation, and to provide a volumetric calculation of gas hydrates and associated free gas. Seismic data show the presence of continuous BSRs in the study area, suggesting that there may be economic potential for gas hydrates offshore southwestern Taiwan.

## Regional geology

Taiwan island evolved in an oblique collision zone between the N-S trending Luzon volcanic arc of the Philippine Sea Plate and the NE-SW trending passive continental margin of the Eurasian Plate since 6.5 Ma (Lin *et al.*, 2003). Offshore southwestern Taiwan (Fig. 1), the Manila subduction system impinges on the rifted continental margin, transforming the subduction system into an incipient arc-continent collision complex in which there is rapid sedimentation and active tectonic deformation. A deformation front separates the rifted continental margin to the west from the fold-and-thrust structures of the accretionary wedge system to the east (Fig. 1). The Western Taiwan foreland basin formed to the west of the orogenic belt as a result of lithospheric flexure due to orogenic loading (Lin and Watts, 2002). During the Pliocene – Holocene, sediments eroded from the Taiwan orogenic belt were transported southwestward and deposited in the foreland basin, in which mud-rich sediments approximately 6000 m

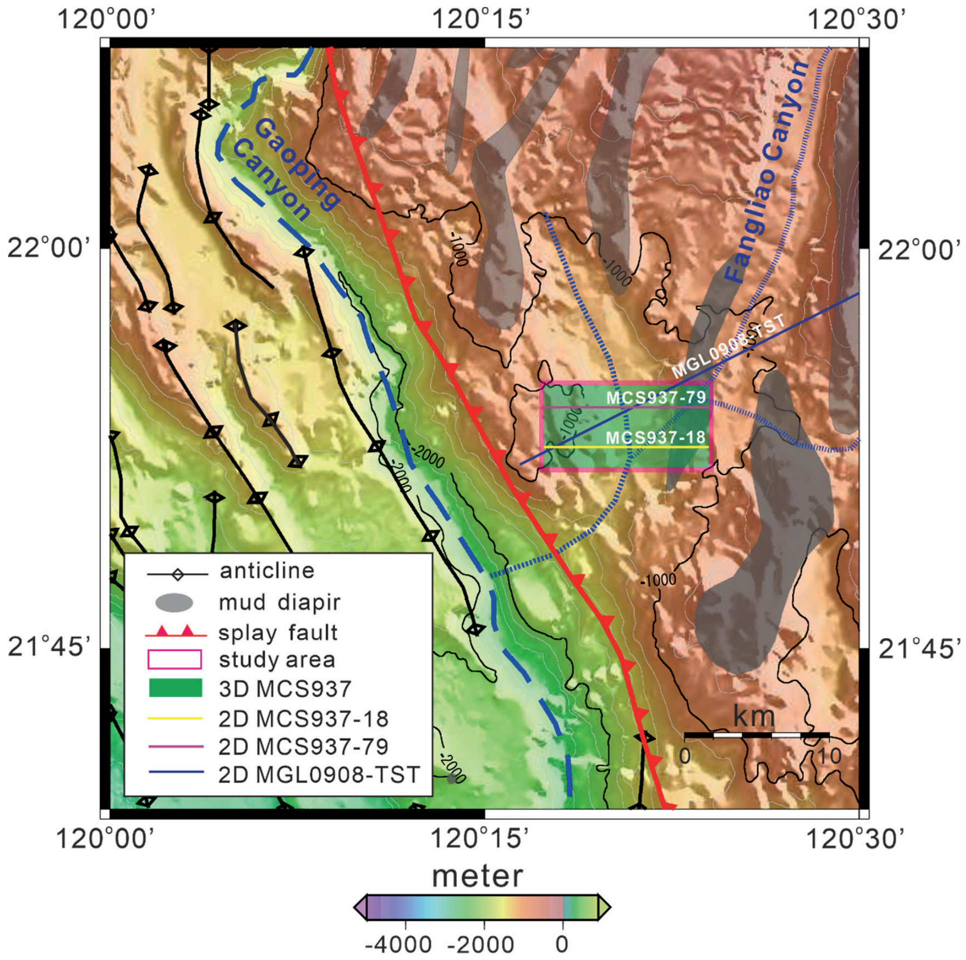


**Fig. 3. Bathymetry and structural elements in the Lower Fangliao Basin, offshore SW Taiwan. Seismic data used in this study are the MCS937 3D seismic volume (shown as the green-shaded rectangular box) and the 2D seismic profiles MGL0908-TST, MCS937-79 and MCS937-18. Structures and mud diapirs are from Lin *et al.*, 2008, 2009a.**

thick accumulated (Covey, 1984). Outgrowth of the submarine accretionary wedge extends westwards to the China continental slope in southwestern offshore Taiwan, where prominent morphological features, include anticlinal ridges and submarine canyons (Liu *et al.*, 2006; Lin *et al.*, 2008; Lin *et al.*, 2009a).

In terms of physiography, offshore southwestern Taiwan can be divided into the Gaoping shelf and the Gaoping slope. The slope extends seaward to about the 3000 m isobath before merging westwards with the northern slope of the South China Sea (Fig. 2) (Chiang *et al.*, 2012; Hsiung *et al.* 2014). Upper and lower slopes are separated by the 1500 m isobath. The Gaoping slope include a rugged seafloor morphology due to the presence of imbricated folds and thrusts together with mud diapirism and deep canyon incisions. NNW-SSE trending ridges pass into NNE-SSW directed ridges in the area near the continental slope. These ridges are the structural extensions of ramp anticlines formed by dominantly west-vergent thrusts in the frontal zone of the accretionary wedge. West-vergent imbricated folds and thrusts occur extensively in the lower slope area, whereas mud diapirs and thrusts dominate the upper slope region. A distinct rise in the seafloor surface between these two slope zones suggests thickening of the accretionary wedge related to uplift on out-of-sequence thrusts (Reed *et al.*, 1992) or splay faults (Lin *et al.*, 2009a).

Along with the Gaoping Canyon, the Fangliao Canyon is one of the two major submarine canyons cutting across the Gaoping slope and is situated to the west of the Hengchun Peninsula (Fig. 2). It starts on the upper slope at 120° 35' E and is generally confined within the active left-lateral strike-slip Fangliao fault zone (Deffontaines *et al.*, 2016), and has no apparent connection to rivers onshore. Yu and Lu (1995) divided the canyon into a relatively straight upper canyon, beginning at the shelf edge and ending approximately at the 600 m isobath; and a lower canyon, extending downslope to about the 1000 m isobath. The canyon mouth lacks a submarine fan and is divided by a north-south trending linear ridge, known as the Fangliao Ridge (Figs 1, 2), which is interpreted to be a consequence of mud diapirism (Yu and Lu, 1995; Lacombe *et al.*, 2004; Chen *et al.*, 2014). Diapiric intrusion in the lower canyon has barricaded the eastern segment, causing the submarine channel to be diverted into the western segment and forming the presentday Fangliao submarine canyon (Chiang *et al.*, 2012, Deffontaines *et al.*, 2016).

Downstream of the Fangliao Canyon is a slope basin, referred to as the Lower Fangliao Basin (Fig. 3), which is an active depositional site for sediments. The basin has emerged since 1.8 Ma (Hsu *et al.*, 2013), and is located near the downslope junction where the Fangliao Canyon merges with the Gaoping Canyon. With average sedimentation rates of 0.7-4.5 mm/year (Lin *et al.*, 2014; Yu *et al.*, 2017), at least 6.6 M tons/yr of sediment have been deposited in the slope basins off southwestern Taiwan (Huh *et al.*, 2009).

Due to the limited nature of previous studies, deep water petroleum exploration in offshore southwestern Taiwan is poorly constrained. To the north and west of the area, petroleum exploration has been concentrated in the shelf of the Tainan Basin (Lee *et al.*, 1993) and the Pearl River Mouth Basin (Zhou and Yao, 2009) (Fig. 1), respectively. Yang *et al.* (2011) viewed the relationship between offshore mud diapirs/mud volcanoes and onshore mud volcanoes as an accretionary wedge conveyor belt. Milkov (2005) and He and Zhou (2018) demonstrated that the development of mud diapirs and mud volcanoes has a close relationship with the distribution of petroleum provinces in frontier areas.

The study area is the offshore continuation of the onshore Pingtung Basin where gas seepages, mud volcanoes and natural gas fields have been found. This paper points to a possible connection between petroleum systems on- and offshore SW Taiwan and the petroleum potential of the study area.

## METHODOLOGY

### Seismic facies analysis

2D and 3D seismic reflection data were used in this study, covering a total line length of more than 1000 km and an area of ~ 60 km$^2$ (Fig. 3). A NE-SW trending 2D seismic profile (MGL0908-TST) was recorded in the study area in 2009 (284 channels, 12.5 m channel spacing and 6 m cable depth). An air-gun array of 6600 cubic inch total volume was towed behind the R/V *Marcus G. Langseth* at a depth of 9 m beneath the sea surface and fired at a 10 second interval, giving a nominal shot interval of 50 m. The 3D seismic data (MCS937) were collected using 84 channels with a 1 ms sampling rate, 25 m channel spacing, 6 m cable depth, 104 in-lines, 1000 cross-lines and 50 m of inline spacing. Shots were fired at 10 second intervals with a nominal shot interval of 12.5 m using an air-gun array with capacity ranging from 150 to 275 cu. in. towed at a depth of 5 m by the R/V *Ocean Researcher I (ORI)* in 2010. Two additional 2D seismic profiles, MCS937-18 and MCS937-79, were extracted from the MCS937 3D seismic volume (Fig. 3).

The seismic surveys were designed to achieve parallel lines crossing the structural trend in the upper slope region. Seismic data were processed at the Institute of Oceanography, National Taiwan University. A typical processing sequence included: trace editing, geometry set-up, band-pass filtering, amplitude compensation, predictive deconvolution, spiking noise removal, velocity analysis, normal move-out correction, stacking, water velocity F–K time migration and water column mute (see details in Hsu *et al.*, 2017).

Seismic facies classifications aim to distinguish areally definable elements using reflection configuration, amplitude, continuity and frequency, and how these elements differ in adjacent facies units (Brown and Fisher, 1982). Seismic stratigraphic interpretation was performed to investigate the influence of mud diapirism on the occurrence of gas hydrates and associated free gas based on seismic facies.

### Seismic geobody extraction

Geobody extraction from 3D seismic data is used to detect facies heterogeneities based on seismic attributes. The trace envelope attribute, also known as the instantaneous amplitude, is an expression of the amplitude envelope of the seismic trace, and can discriminate major lithology changes and unconformities (Taner *et al.*, 1994; Bahk *et al.*, 2013). Together with phase information, the envelope attribute is used to delineate free gas and gas-hydrate bodies. Under the envelope attribute, the seismic amplitudes can be expressed in terms of an opacity level. The spatial distribution of geobodies was generated using an opacity rendering technique. The designated opacity threshold was then used to derive an approximation of the gross rock volume by automatic pattern recognition for both gas-hydrate and free gas prospects. Thus geobody extraction attempted to mitigate the absence of exploration wells within the study area.

### Volumetric estimation

A volumetric estimation provides a static measure of the hydrocarbons in place. Analogous to conventional petroleum estimation, the original volumes of gas hydrates in-place (*OGHIP*) and the original free gas in-place (*OFGIP*) were determined (Fig. 4) and were defined as follows:

$$OGHIP = A.\ H.\ N/G.\ \Phi.\ S_{gh}.\ VR.\ CO.\ (1/28.3) \qquad (1)$$

$$OFGIP = A.\ H.\ N/G.\ \Phi.\ S_{fg}.\ (1/B_g).\ (1/28.3) \qquad (2)$$

where *A* is the areal extent of potential gas hydrates or free gas (km$^2$); *H* is the gross thickness of possible gas hydrates or free gas occurrence (m); *N/G* is the ratio of the thickness of gas hydrates (or free gas) to the gross

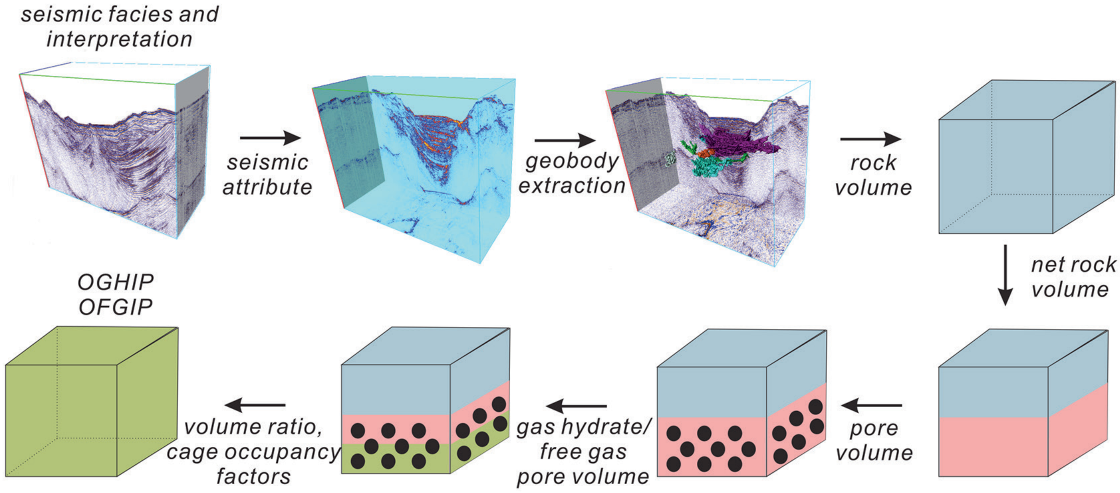


**Fig. 4. Schematic diagrams of in-place gas resource assessment. Three-dimensional reservoir extent is calculated based on geobody volume extraction. *OGHIP*: original gas hydrates in-place; *OFGIP*: original free gas in-place.**

thickness; $\varphi$ is porosity; $S_{gh}$ and $S_{fg}$ are the saturation of gas hydrates and free gas, respectively; *VR* is the volume ratio of gas hydrates and natural gas converted from hydrates (172 at 0 °C and 1 atm); *CO* is the cage occupancy of methane occupied in hydrates; $B_g$ is the gas formation volume factor; and 1/28.3 is a conversion unit to Bcf (billion cubic feet) (1 Bcf = 28.3 M $m^3$).

Despite the absence of hydrate-bearing core samples in the study area, recent geophysical studies have attempted to evaluate the petrophysical properties needed for volumetric estimations, such as the hydrate-free gas saturation based on electromagnetic studies (Hsu *et al.*, 2014), porosity-depth relationships (Lin *et al.*, 2003) and drilling results from adjacent gas-hydrate exploration wells in the Nankai Trough (Fujii *et al.*, 2009).

The area and gross thickness were defined based on the geobody extraction from the 3D MCS937 seismic volume, and were converted into depths by applying the time-depth conversion function from Lin *et al.* (2014). Probabilistic estimation based on Monte Carlo simulation was then performed to manage the uncertainty in the input parameters. A similar approach has been used to evaluate gas-hydrate prospects in the Gulf of Mexico (Majumdar and Cook, 2018) and the Ulleung Basin (Riedel *et al.*, 2013).

The statistical distribution of each parameter was set to a range of possible values used in the stochastic calculation. Estimate percentiles (e.g. P10, P50 and P90) were used to denote the probabilities of given reservoir properties being calculated under a given forecast uncertainty range. Based on Central Limit Theorem, the P50 is deemed to have more chance of occurring than the P10 and P90 estimates; thus P50 was selected as the most appropriate probability in this study.

As OFGIP estimation follows the conventional estimation of original gas-in-place approach, one of the key parameters in equation 2 is $B_g$, the gas formation volume factor. Its value is dependent on pressure, temperature (in the Rankine scale, °R), gas composition and reservoir conditions. $B_g$ relates the gas volume at reservoir conditions to the volume at standard conditions, and is described as follows:

$$B_g = \frac{V_r}{V_s} = \frac{P_s n Z R T_r}{P_r n Z_s R T_s} = \frac{Z T_r P_s}{P_r T_s} \qquad (3)$$

where $V_r$ is the gas volume under reservoir conditions; $V_s$ is the gas volume at surface conditions; $P_s$ is standard atmospheric pressure (14.7 psi); $P_r$ is reservoir pressure (psi); $n$ is the amount of the gas (moles); $Z$ is the gas compressibility factor; $Z_s$ is the standard gas compressibility factor (= 1); $R$ is the gas constant (8.31441 $J.K^{-1}.mol^{-1}$); $T_r$ is temperature at reservoir conditions (°R); and $T_s$ is temperature at surface conditions (= 520 °R).

Equation 3 includes three non-constant parameters ($Z$, $P_r$ and $T_r$). For a non-ideal gas, $Z$ can be calculated under the gas critical point based on thermodynamic equations of state from Peng *et al.* (1976), known as the Peng-Robinson equation, as follows:

$$P = \frac{RT}{\upsilon - b} - \frac{a\ (T)}{\upsilon(\upsilon + b) + b(\upsilon - b)} \qquad (4)$$

where $P$ is the pressure (psi); $T$ is absolute temperature (°K); $a$ is the attraction parameter; $\upsilon$ is molar volume ($m^3$/mol); and $b$ is van der Waals volume ($m^3$/mol). Elliot and Lira (1996) solved the Peng-Robinson equation for $Z$ under given gas critical constants, acentric factor, pressure and temperature constraints. In order to derive reservoir pressure, Hamilton's (1980) estimation of sub-bottom depths based on seismic travel times is implemented and is described as follows:

$$D = 1{,}511\ t + 1{,}041\ t^2 - 372\ t^3 \qquad (5)$$

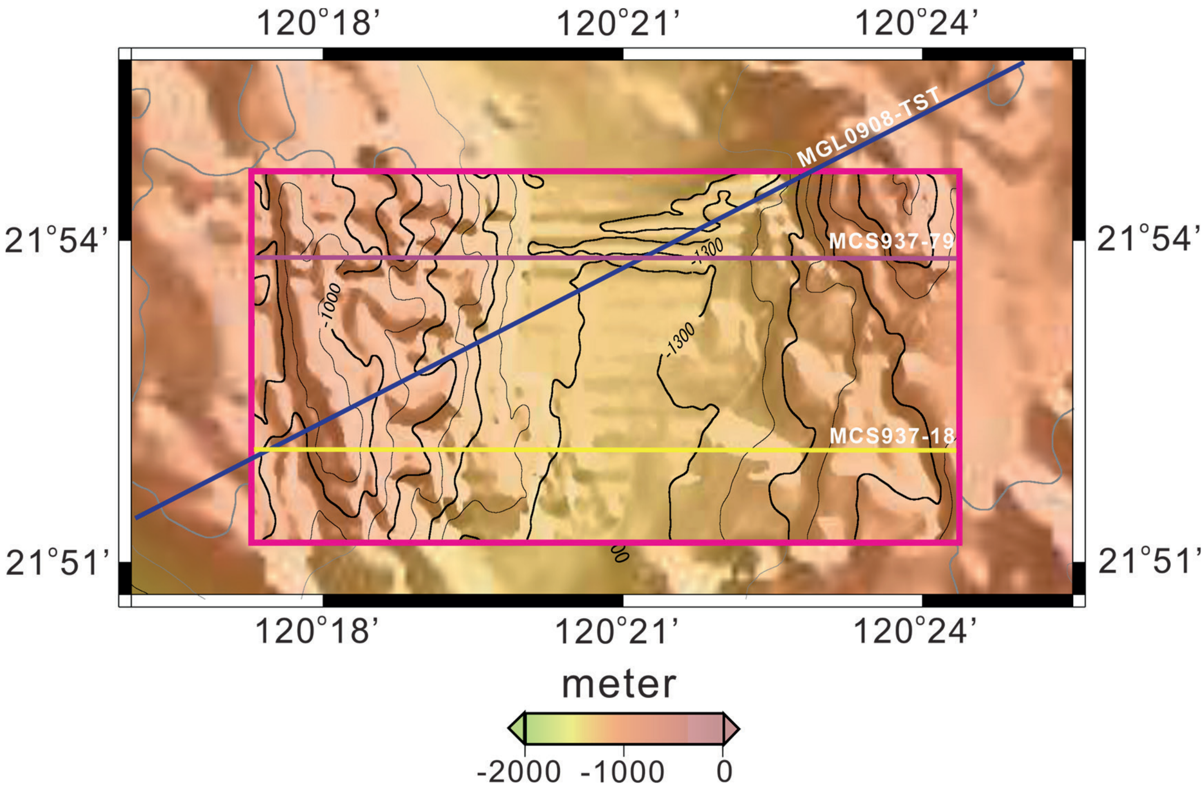


**Fig. 5. High resolution seafloor image from the MCS937 3D seismic volume (pink square) superimposed on bathymetry data. Profiles of the three interpreted seismic lines, MGL0908-TST, MCS937-79 and MCS937-18 are shown by the dark blue, purple and yellow-coloured lines, respectively; the interpreted profiles are presented in Figs 7, 8 and 9.**

where $D$ is the depth of interest (m); $t$ is one-way travel time below the seafloor (s). This relationship has been used in previous studies offshore SW Taiwan (Chi *et al.*, 1998; Schnurle *et al.*, 1999; Liu *et al.*, 2006; Chi and Reed, 2008).

Since gas hydrates and associated free gas accumulations are located at relatively shallow depths, the reservoir pressure is assumed to be constrained mainly by overburden pressure, $P_r$, and can be estimated as follows:

$$P_r = \rho_w g\, y + \rho_w Z_{BSR} + P_0 \qquad (6)$$

where $\rho_w$ is the water density (kg.m$^{-3}$); $g$ is the standard gravity constant (9.8 m.s$^{-2}$); $\rho$ is the sediment density above BSRs (kg.m$^{-3}$); and $P_o$ is the atmospheric pressure (psi). Considering that the upper slope of the accretionary wedge is dominated by clays, the water density and bulk sediment density were assumed to be 1025 kg.m$^{-3}$ and 1700 kg.m$^{-3}$, respectively (Shyu *et al.*, 2006).

In the study area, a relatively low geothermal gradient (33 $^o$C/km) based on BSR-controlled heat-flow estimations, was proposed by Dirgantara *et al.* (2019, *in press*). Assuming a linear geothermal gradient, this value was used and extrapolated to derive the temperature at reservoir depths.

## RESULTS

### Morphology

A high-resolution bathymetric map of the study area derived from seafloor picking of the 3D seismic volume indicates that the Lower Fangliao Basin has an average water depth of ~ 1300 m and an average width of ~ 4000 m (Fig. 5). It is bounded by submarine ridges with average water depths of ~ 1000 m. The western ridge is relatively shallower than its eastern counterpart and at its shallowest point reaches a water depth of ~ 700 m. Hsiung *et al.* (2014) suggested that the basin is confined to, and has developed within, an intraslope topographic depression wedged between mud diapiric ridges. The depth of the basin increases toward the south.

A 3D image of the study area shows the influence of mud diapirs on the structure of the intraslope basin (Fig. 6). Mud diapirs can be recognised on strike-aligned seismic reflection profiles as acoustically-transparent piercement structures (Figs 7, 8, 9), and the profiles show that the Lower Fangliao Basin is flanked by mud-diapiric ridges on either side. A local depression is visible at the summit of a buried mud diapir in Fig. 7. Fault-induced diapirs can be seen as vertical blanking zones at the flanks of the diapir body (Fig. 8). In the basin depocentre, a mud diapir intrudes up to near the seafloor (Fig. 9). The seismic

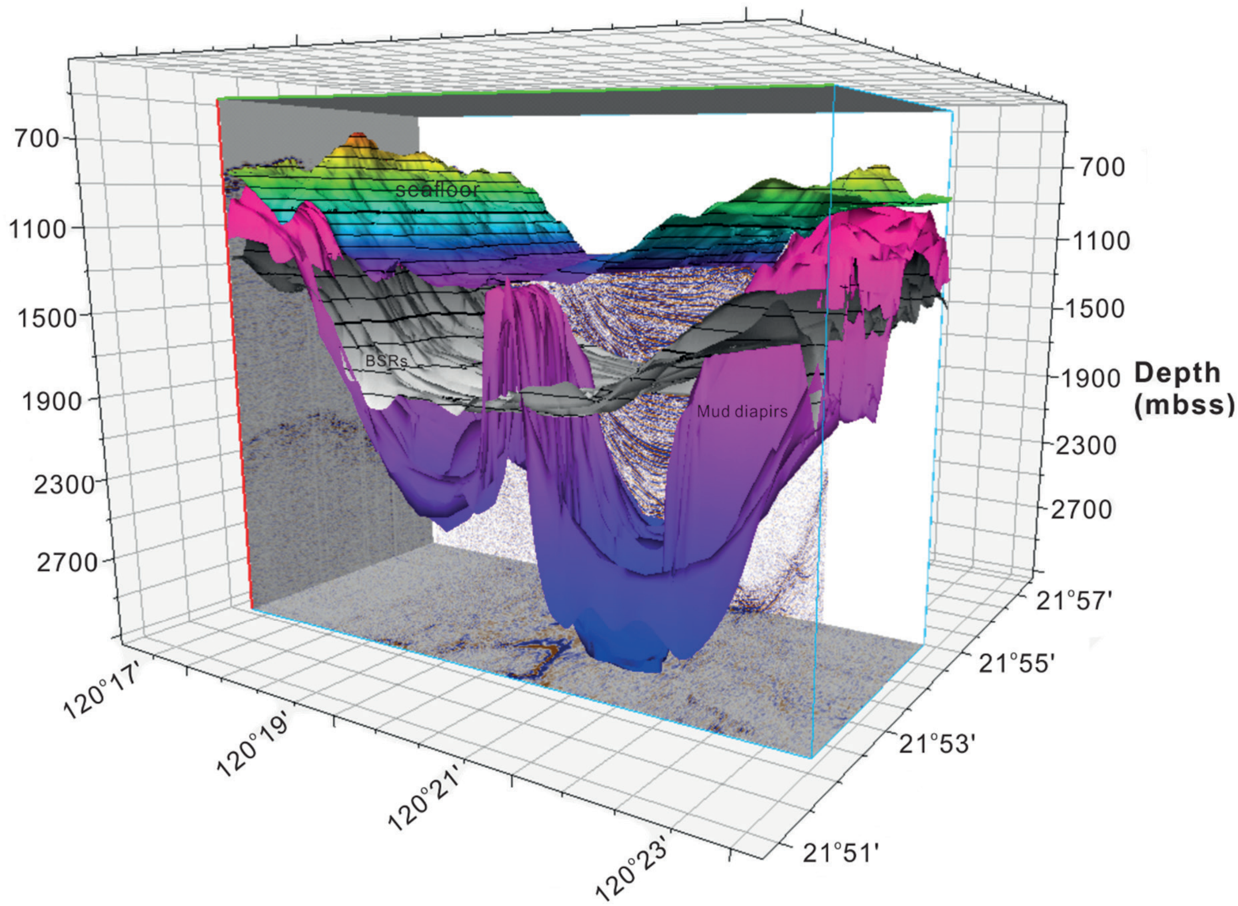


**Fig. 6. 3D block diagram combining three-dimensional seafloor bathymetry, BSRs and mud diapirs. BSRs are clearly imaged across the mud diapirs. Abbreviation: mbss: metres below sea surface.**

internal reflections of both ridges are nearly vertical and sub-transparent in some parts, while stacked channels between the mud diapirs with channel-infills are present (Figs 7, 8, 9).

## Seismic facies

Five seismic facies were identified in profiles (Figs 7, 8, 9) across the study area (Table 1). Facies A in general consists of stratified, parallel to sub-parallel, low-amplitude reflections. This facies dominates the uppermost portion of the sedimentary column and the lack of disturbance suggests hemipelagic sedimentation (e.g. Basov *et al.*, 1996). Facies B represents intervals of semi-transparent, internally contorted and discordant reflections interpreted as mass-transport deposits (MTDs) (Sangree and Widmier, 1978). Facies C is characterised by stacked, high-amplitude bowl-shaped reflections, best interpreted as cut-and-fill channels confining turbidite sands. Facies D at the base of the basin fill consists of continuous, convex-shaped reflections whose edges off- and onlap the flanks of mud diapirs. These relatively conformable reflections indicate deposition prior to mud intrusion, e.g. overbank sediments. Facies E is defined by transparent, stacked dome-shaped reflections at the flanks of mud diapirs interpreted as drag features caused by the mud intrusion.

## BSR characteristics

BSRs are present throughout the Lower Fangliao Basin, where they cross-cut inclined seismic reflections and intruding mud diapirs (Figs 7, 8, 9). Primary BSRs are assumed to mark the basal phase boundary of the gas hydrate stability zone (GHSZ) and are relatively parallel to seabed relief. The nature of the reversed-polarity BSRs relative to that of seafloor reflections suggests higher acoustic impedance strata overlying lower acoustic impedance strata across the BSRs, suggesting possible gas hydrates overlying free gas accumulations. In addition, strong reversed polarity reflections above BSRs are also present, indicating that free-gas pockets within the GHSZ (Figs 9, 10) are feasible.

In the study area, the amplitudes of the BSRs are variable; most BSRs show high-amplitude reversed-phase reflections, while others exhibit low amplitude signatures. Some of the BSRs are continuous and can easily be traced in seismic profile (Fig. 7), but others do not necessarily follow this general pattern (Figs 8, 9). Although the presence of BSRs indicates the likely occurrence of gas hydrates, the reverse argument is not valid. Well data from the Gulf of Mexico (Brooks *et al.*, 1988), the Black Sea (Soloviev and Ginsburg, 1994) and the Blake Ridge (Holbrook, 2000) show

**Table 1. Illustration of the five seismic facies and possible associated sedimentary features identified in the Lower Fangliao Basin.**

| Type | Seismic facies | Reflectivity configuration, amplitude and continuity | Interpretation |
|---|---|---|---|
| A | 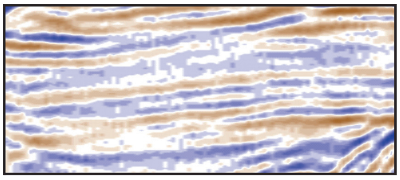 | Stratified, parallel to sub-parallel and low-amplitude reflections | Hemipelagic sediments |
| B | 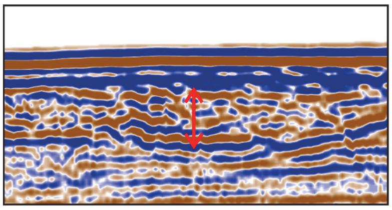 | Chaotic or contorted reflections | Mass-transport deposits |
| C | 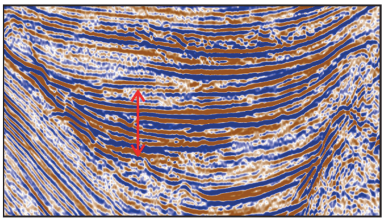 | Semi parallel, high amplitude reflections | Cut-and-fill turbidite sands |
| D | 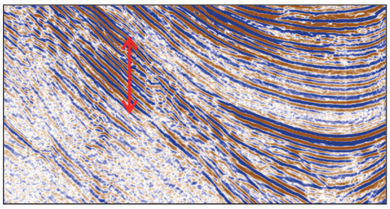 | Oblique, semi-continuous and high amplitude reflections | Overbank sediments |
| E | 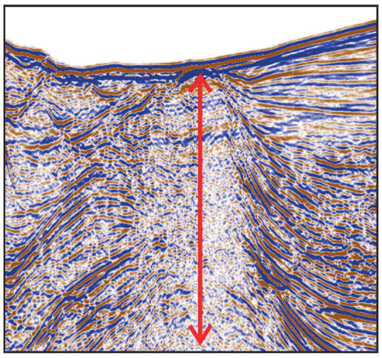 | Dome shaped and transparent reflections | Mud diapirs |

that gas hydrates are not necessarily accompanied by BSRs. This suggests the possibility that gas hydrates are present even in areas where the response of the BSRs is relatively weak or non-existent.

### Geobody extraction

Although visible on conventional seismic sections, amplitude anomalies are more apparent on attribute sections. Fig. 11 shows both conventional seismic and envelope attribute sections together to highlight anomalies in the study area. In Fig. 11a, a blanking zone above the BSRs is present, indicating the presence of gas hydrates. Enhanced reflections are observed below the blanking zone, implying the occurrence of free gas below the GHSZ. As shown in Fig. 11b, BSRs cut across enhanced reflections, suggesting possible free gas accumulations beneath the stability zone. Draping enhanced reflections above BSRs may terminate against the flanks of mud diapirs (Fig. 11c).

### Reservoir parameters

Due to the absence of drilling, reservoir coverage is derived from the spatial extent of BSRs-defined area based on geobody extraction (Fig. 12). According to the above-mentioned characteristics of the BSRs, potential prospects in the study area can be divided into

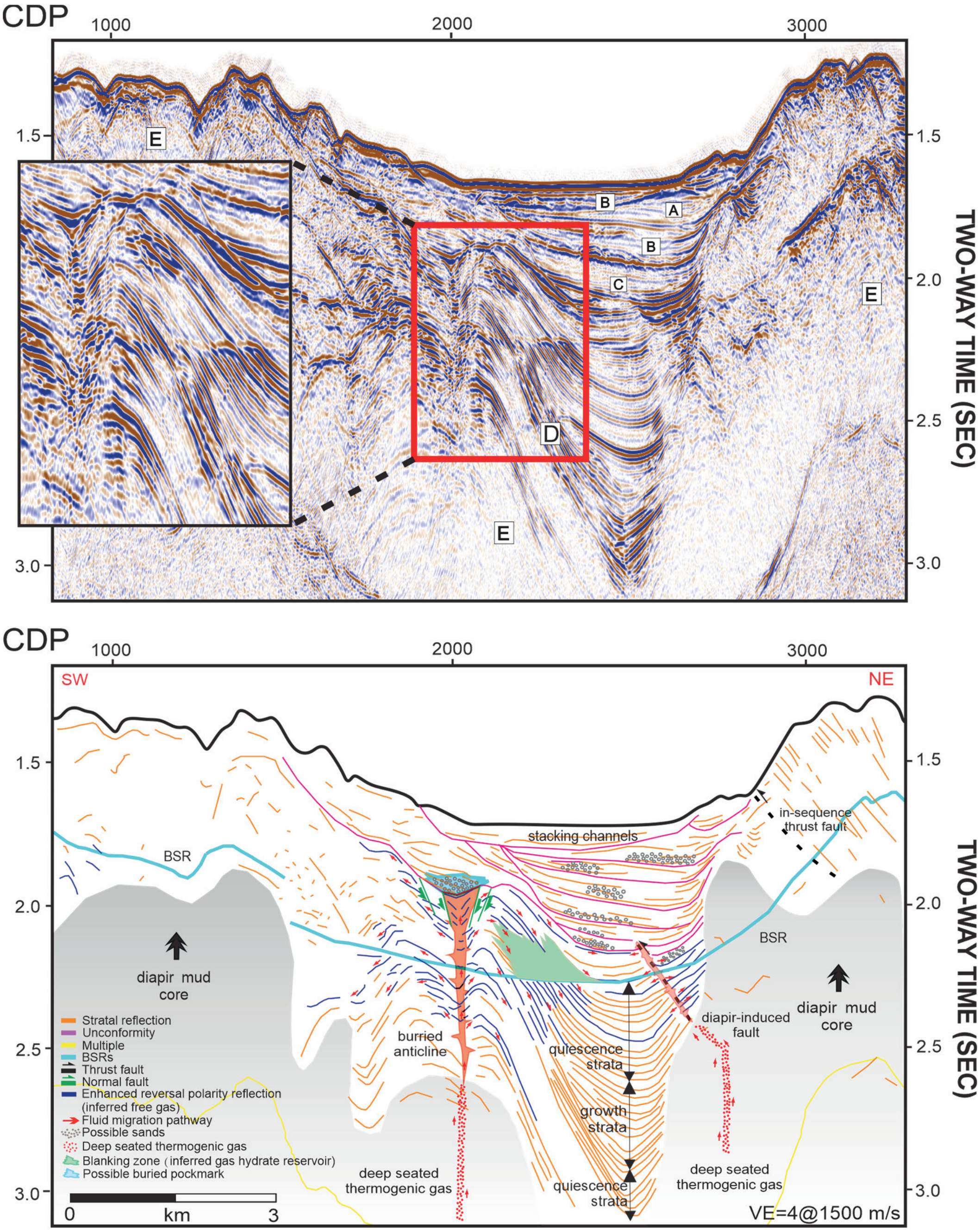


**Fig. 7. Uninterpreted (above) and interpreted (below) reflection seismic data from the MGL0908-TST 2D line. Inset at upper left is an enlarged part of the uninterpreted profile (red square), showing collapsed and buried mud diapiric anticline. A possible buried pockmark above the collapsed anticline indicates upward migration of fluids along the structure. Abbreviations: CDP, common depth points; VE, vertical exaggeration. Letters in the uninterpreted figure indicate facies types (see Table 1).**

three categories, namely: (i) gas-hydrate compartments above BSRs (17.60 km$^2$) in Fig. 12a; (ii) free gas compartments above BSRs (1.71 km$^2$) in Fig. 12b; and (iii) free gas compartments below BSRs (14.67 km$^2$) in Fig. 12c.

The thickness of each prospect was converted from time to depth based on Lin *et al.* (2014), giving average thicknesses of 436.10 m, 341.21 m and 445.57 m respectively for gas-hydrate compartments above BSRs, free gas compartments above BSRs and free gas compartments below BSRs.

Assuming reservoirs are confined to high-porosity intervals (e.g. Facies B and C: Table 1), *N/G* (net-to-gross) values range from 0.1 to 0.4 following previous studies (e.g. Fujii *et al.*, 2009) of locations in which the sedimentary and tectonic settings are similar to those in the study area. The porosity-depth relationship for Cenozoic sediments in western and southwestern Taiwan from Lin *et al.* (2003) was used as a proxy for porosity values, with an estimated range of 0.3-0.4. Previous estimates of gas-hydrate and free gas saturations in offshore southwestern Taiwan based on

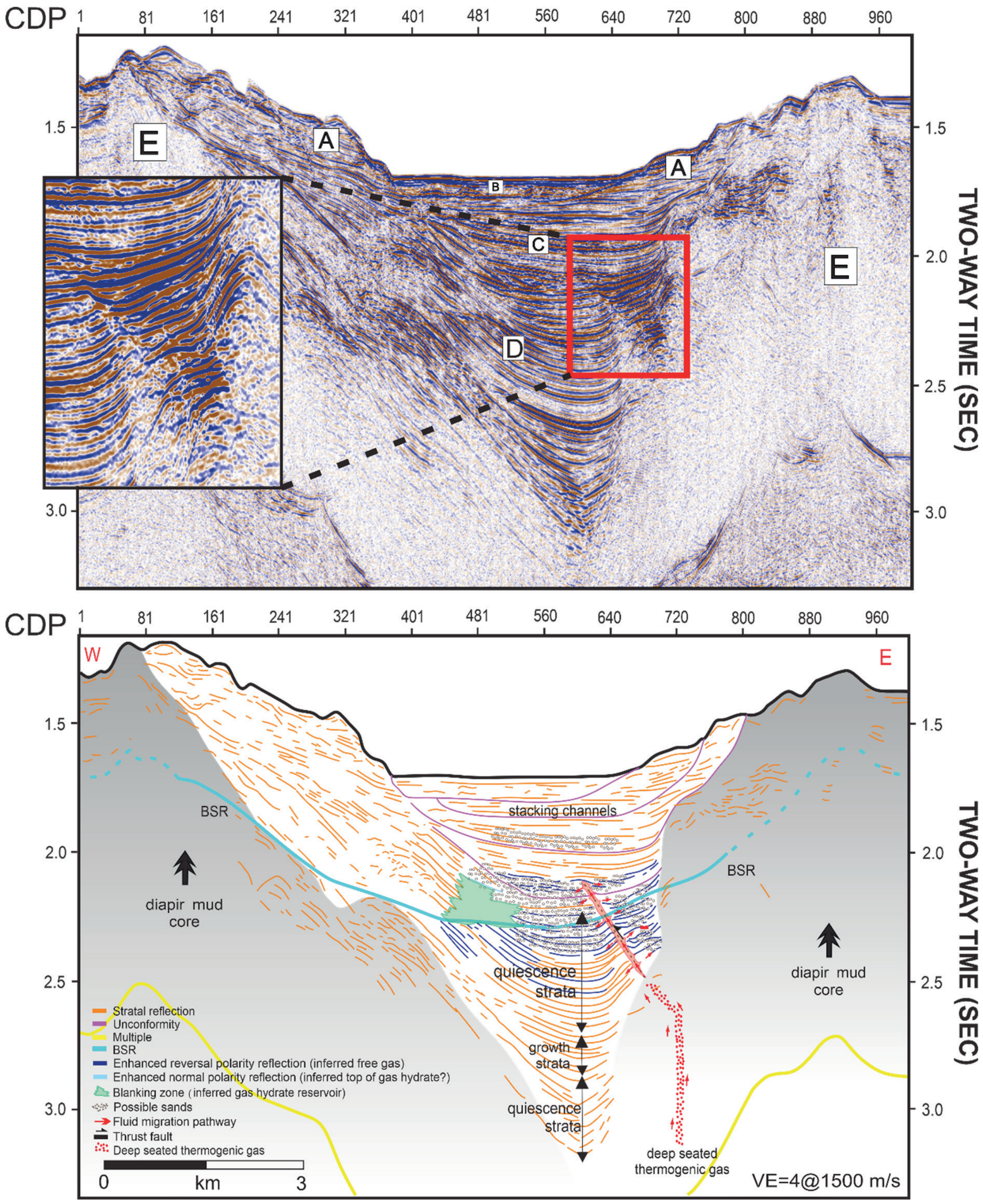


**Fig. 8. Uninterpreted (above) and interpreted (below) reflection seismic section from the MCS937-79 2D line. Inset is an uninterpreted and enlarged profile showing enhanced seismic reflections in the area marked by the red square, indicating free gas -charged sediments. Deep-seated thermogenic gas is inferred to have migrated upwards through fault-induced conduits in the mud diapir. The presence of both normal strata and growth strata is a response to the dynamics of mud diapirism through time (see text for details). Abbreviations: CDP, common depth points; VE, vertical exaggeration. Letters in the uninterpreted figure indicate facies types (see Table 1).**

geophysical measurements (Wu *et al.*, 2007; Cheng *et al.*, 2010; Hsu *et al.*, 2014) suggested saturations ranging from 0.13 to 0.35. Volume ratio, *VR*, is set as a constant of 172 under conditions of 0 °C and 1 atm (Collett, 1997). The value of the cage occupancy, *CO*, is based on drilling results and the analyses of hydrate samples in previous studies (Fujii *et al.*, 2009), and is 0.9-1.

The gas formation volume factor and gas compressibility were calculated from the average depth and predicted reservoir temperatures from each reservoir. Based on time-to-depth conversion, a linear geothermal gradient (Dirgantara *et al.*, 2019, *in press*) and constant overburden pressure (Eq. 5), average values for reservoir depth, temperature and pressure were estimated as follows: 1306 m, 568.8 °R and 2285 psi for free gas compartments above BSRs; and 1837 m, 599.4 °R and 3472 psi for free gas compartments below BSRs.

Considering that the gas component in the hydrates offshore Taiwan is dominated by methane (Schnurle *et al.*, 2004; Chi and Reed, 2008), the critical pressure

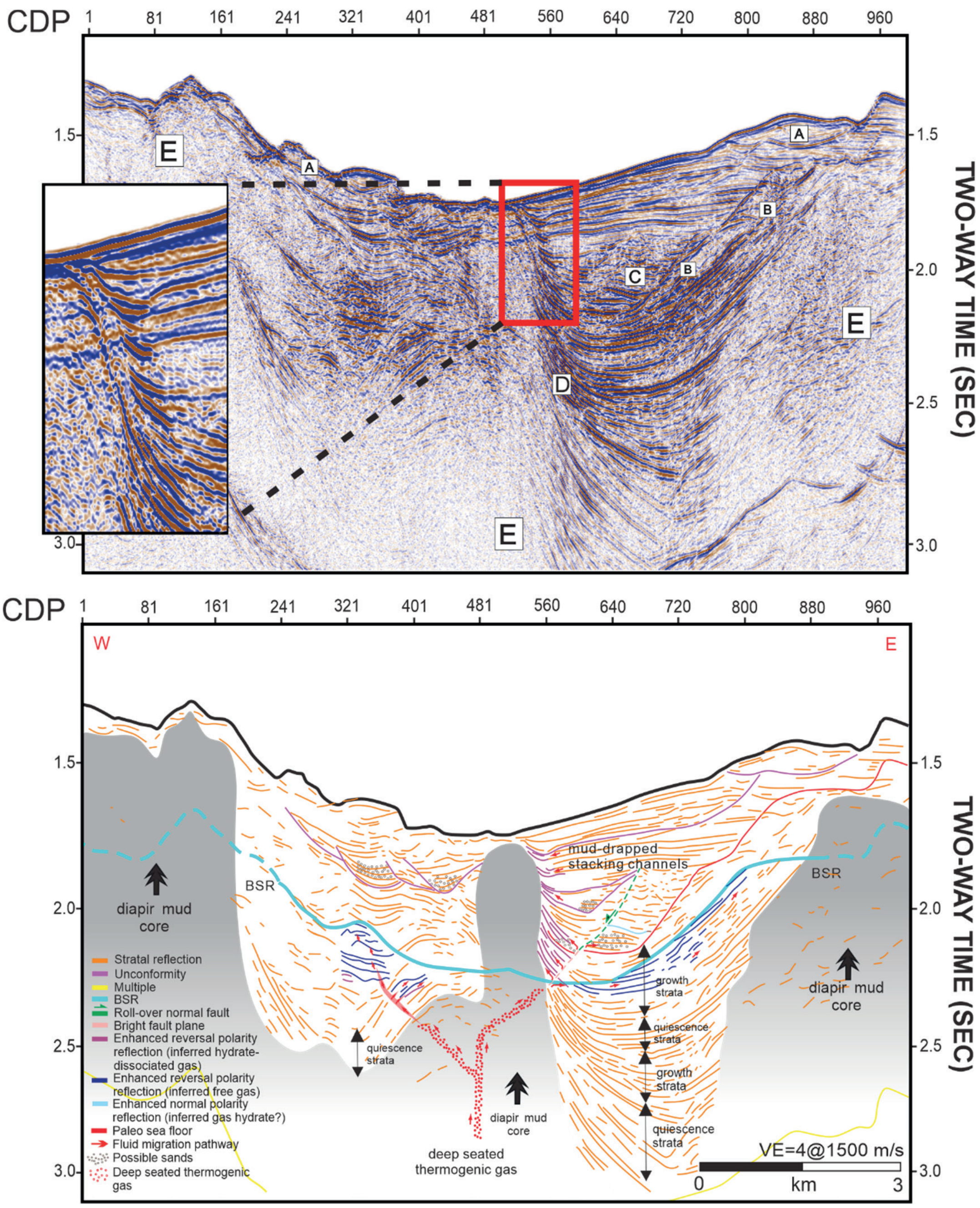


**Fig. 9. Uninterpreted (above) and interpreted (below) reflection seismic profile from the MCS937-18 2D line. The inset, uninterpreted figure is an enlargement profile (red square), showing dragged reflections on the diapiric flank with reversal polarity. Similar reflection characteristics are seen below the BSRs. Abbreviations: CDP, common depth points; VE, vertical exaggeration. Letters in the uninterpreted figure indicate facies types (see Table 1).**

and temperature are set as 4.60 MPa and 190.6 °K, respectively (Elliot and Lira, 1996).

These inputs were then incorporated into Eq. 4, deriving Z values of 0.839 and 0.891 for free gas compartments above and below BSRs, respectively. By introducing pressure and reservoir temperature conditions for each reservoir into Eq. 3, *Bg* values were estimated as 0.005892 and 0.004339 for free gas compartments above and below BSRs, respectively. Since gas compressibility is the inverse product of gas formation volume factor, 1/*Bg* values were determined as 169.73 for free gas compartments above BSRs, and 230.47 for free gas compartments below BSRs. Details regarding the input parameters for the calculation of gas formation volume factor and gas compressibility are shown in Table 2.

Each reservoir parameter is defined by a range of possible values used in stochastic models based on the Monte Carlo method under 1,000,000 iterations (Fig. 13). For first-order estimates, this method is efficient for dealing with high degrees of uncertainty (Majumdar and Cook, 2018). A compilation of reservoir parameters

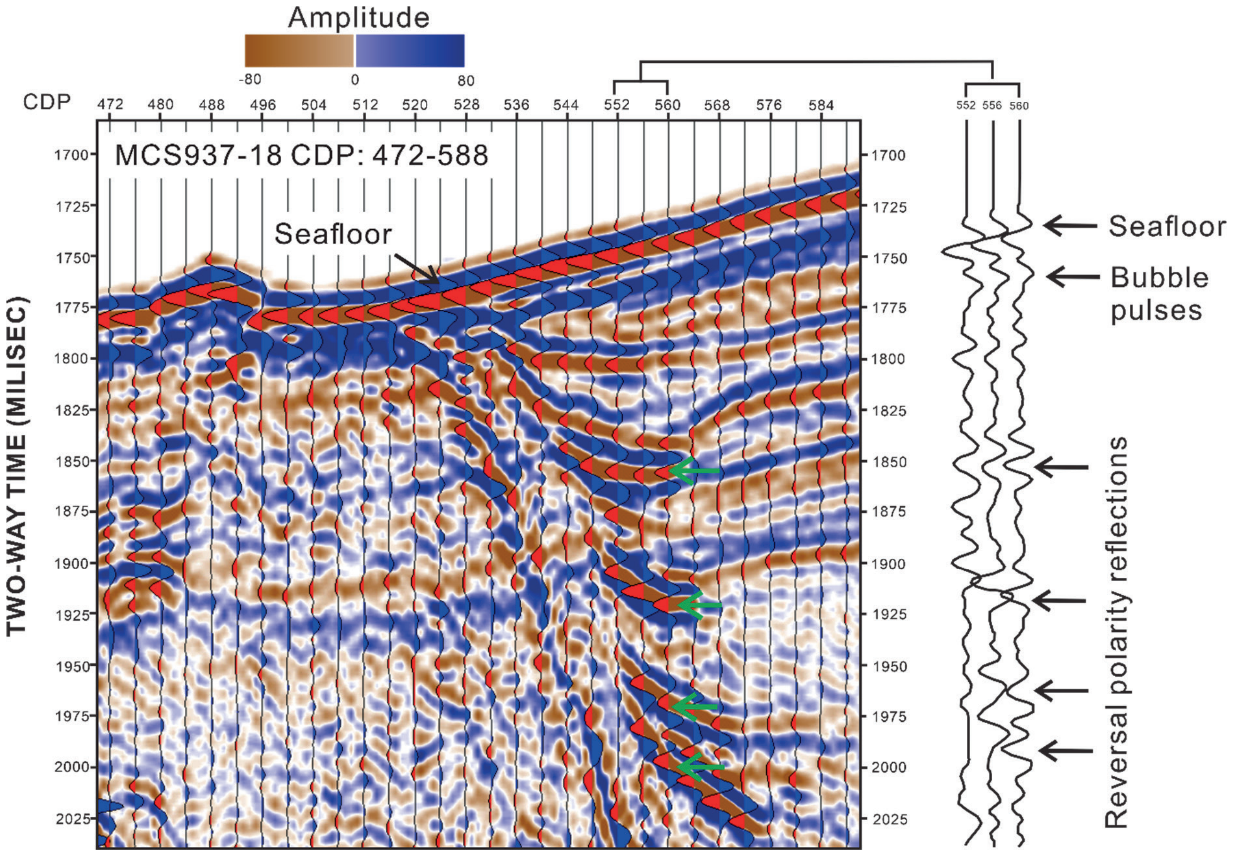


**Fig. 10. A segment of seismic profile MCS937-18 in the study area, showing enhanced reflections draping on the dome-shaped reflections (green arrows). Amplitudes with blue colour represent positive reflection coefficients, and those with red colour indicate negative reflection coefficients. The extracted wavelets on the right show seismic amplitudes and associated interpretations. Note that the phase of the enhanced reflections is reversed relative to that of the seafloor.**

used in defining in-place hydrocarbon volumes is presented in Table 3. The range of uncertainty of the potential volume is represented by a probability distribution (Fuji *et al.*, 2009). Depending upon the number of uncertainties and the ranges specified for each parameter, the Monte Carlo method is capable of producing a distribution of possible outcome values.

## DISCUSSION

### Gas-hydrate and free gas systems

The extensive distribution of BSRs recorded from seismic reflection data in the Lower Fangliao Basin suggests the existence of widespread gas-hydrate and free gas systems in the area. The growth of mud diapirs in the study area is ascribed to compressional tectonic forces, overpressuring and the presence of gas-bearing fluids (Yu and Lu, 1995; Chen *et al.*, 2014), and has resulted in the distinct sea floor morphology. In general, the mud diapirs in the Gaoping slope are overlain by younger sediments, although in some areas diapirs have pierced to the seafloor, e.g. in the Fangliao Canyon area (Chen *et al.*, 2014).

Hemipelagic sediments (Facies A: Table 1) dominate the uppermost parts of the sedimentary pile. Considering that the location of the basin is proximal to Taiwan island, these sediments may consist mostly of terrigenous sediments. High amplitude and non-continuous reflections with an analogous phase to that of the seafloor may indicate the likelihood of porous turbidite sandstones (Facies C). Increasing burial depths cause an increase in compaction stresses and temperature, resulting in a decrease in porosity and initiating thermal maturation of organic matter (Tissot and Welte, 1984). In areas with rapid sedimentation, overpressured and plastically-deformed muds may slowly ascend through overburden rocks and faults as diapirs (Facies E). The pervasive distribution of MTDs (Facies B) suggests periodic episodes of submarine landslides within the basin. Large-scale submarine landslides have been identified in the west of the Hengchun Peninsula, including the Fangliao Canyon (Deffontaines *et al.*, 2016). At greater depths in the basin (beginning from ~ 2.2 second TWT), thick and continuous oblique reflections are discernible (Facies D) and indicate the deposition of overbank sediments.

Owing to changes in impedance contrast, the presence of BSRs is indicated by reversed polarity reflections which mimic the seafloor relief and which cut across the stratigraphy, including the diapiric

**Table 2. Range of parameters used in defining the gas compressibility and gas formation volume factor (FVF).**

| Area | Reservoir depth (m) | Reservoir pressure (psi) | Reservoir temperature (º Rankine) | Gas compressibility | Gas FVF |
|---|---|---|---|---|---|
| Free gas above BSRs | 1,306 | 2,285 | 568.8 | 0.839 | 0.005892 |
| Free gas below BSRs | 1,837 | 3,472 | 599.4 | 0.891 | 0.004339 |

**Table 3. Range of reservoir parameters used in defining the in-places volumes of hydrate-bound methane.**

Gas-hydrate compartments above BSRs

| Parameter | Distribution type | Range value |
|---|---|---|
| Area (*km*$^2$) | Triangular | 15.84 : 17.60 : 19.37 |
| Thickness (*m*) | Log normal | $\bar{x}$ = 436.10, σ = 10.0 |
| Net/gross | Log normal | $P_{10}$ = 0.20, $P_{90}$ = 0.40 |
| Porosity | Log normal | $P_{10}$ = 0.36, $P_{90}$ = 0.39 |
| Hydrate saturation | Log normal | $P_{10}$ = 0.22, $P_{90}$ = 0.35 |
| Volume ratio | Constant | 172 |
| Cage occupancy | Triangular | 0.90 : 0.95 : 1.00 |

Free gas compartments above BSRs

| Parameter | Distribution type | Range value |
|---|---|---|
| Area (*km*$^2$) | Triangular | 1.539 : 1.710 : 1.881 |
| Thickness (*m*) | Log normal | $\bar{x}$ = 341.22, σ = 10.0 |
| Net/gross | Log normal | $P_{10}$ = 0.20, $P_{90}$ = 0.40 |
| Porosity | Log normal | $P_{10}$ = 0.36, $P_{90}$ = 0.40 |
| Gas saturation | Log normal | $P_{10}$ = 0.18, $P_{90}$ = 0.25 |

Free gas compartments below BSRs

| Parameter | Distribution type | Range value |
|---|---|---|
| Area (*km*$^2$) | Triangular | 13.21 : 14.67 : 16,14 |
| Thickness (*m*) | Log normal | $\bar{x}$ = 5.10, σ = 1.0 |
| Net/gross | Log normal | $P_{10}$ = 0.20, $P_{90}$ = 0.40 |
| Porosity | Log normal | $P_{10}$ = 0.30, $P_{90}$ = 0.31 |
| Gas saturation | Log normal | $P_{10}$ = 0.13, $P_{90}$ = 0.18 |

ridges (Fig. 6). The 180º phase shift caused by the decreasing interval velocity beneath the BSRs results in a strong acoustic impedance response. Since the presence of low-level free gas in pore spaces causes the significant decay of P-wave velocity (Chi *et al.*, 1998; Lin *et al.*, 2009b), the polarity reversal suggests higher impedance gas hydrates -hosted layers overlying lower impedance layers with free gas. Blanking zones above BSRs are attributed to a reduction of porosity due to a low to modest gas-hydrate saturation, while a modest to high gas-hydrate saturation leads to strong, positive amplitudes (Figs 7, 8).

In the absence of exploration drilling, the lithological nature of gas-hydrate reservoirs in the study area remains unknown. Previous studies have reported a wide spectrum of gas-hydrate reservoirs from pore- and fracture-filling mudstones (Riedel *et al.*, 2010; Lee and Collet, 2012) to sandstones interbedded with conglomerates (Collet *et al.*, 2009; Yamamoto *et al.*, 2015). Without ruling out alternative possibilities, however, the cut-and-fill facies was interpreted by previous studies as remnant deposition from the paleo-Gaoping canyon (Sun and Liu, 1993; Hsu *et al.*, 2017; Dirgantara *et al.*, 2019 *in press*), suggesting sandy turbidite deposition.

Enhanced reflections with reversed polarity flanking the mud diapirs also occur in areas above BSRs, indicating the presence of possible free gas (Figs 9, 10). While the presence of the GHSZ is mainly controlled by pressure and temperature, a high proportion of methane, greater than the solubility of methane in water, is a prerequisite for the formation of gas hydrates in the GHSZ (Sloan, 1998). The limited amount of water required to trap methane within the hydrate crystals contributes to the presence of free gas rather than gas hydrates, causing the impedance contrast to be more obvious, and results in reflection enhancement. Shyu *et al.* (1998) suggested that anomalous temperatures and thermal gradients are present above mud diapirs near the Fangliao Ridge. The high thermal conductivity of diapirs locally elevates the surrounding thermal gradients, causing them to

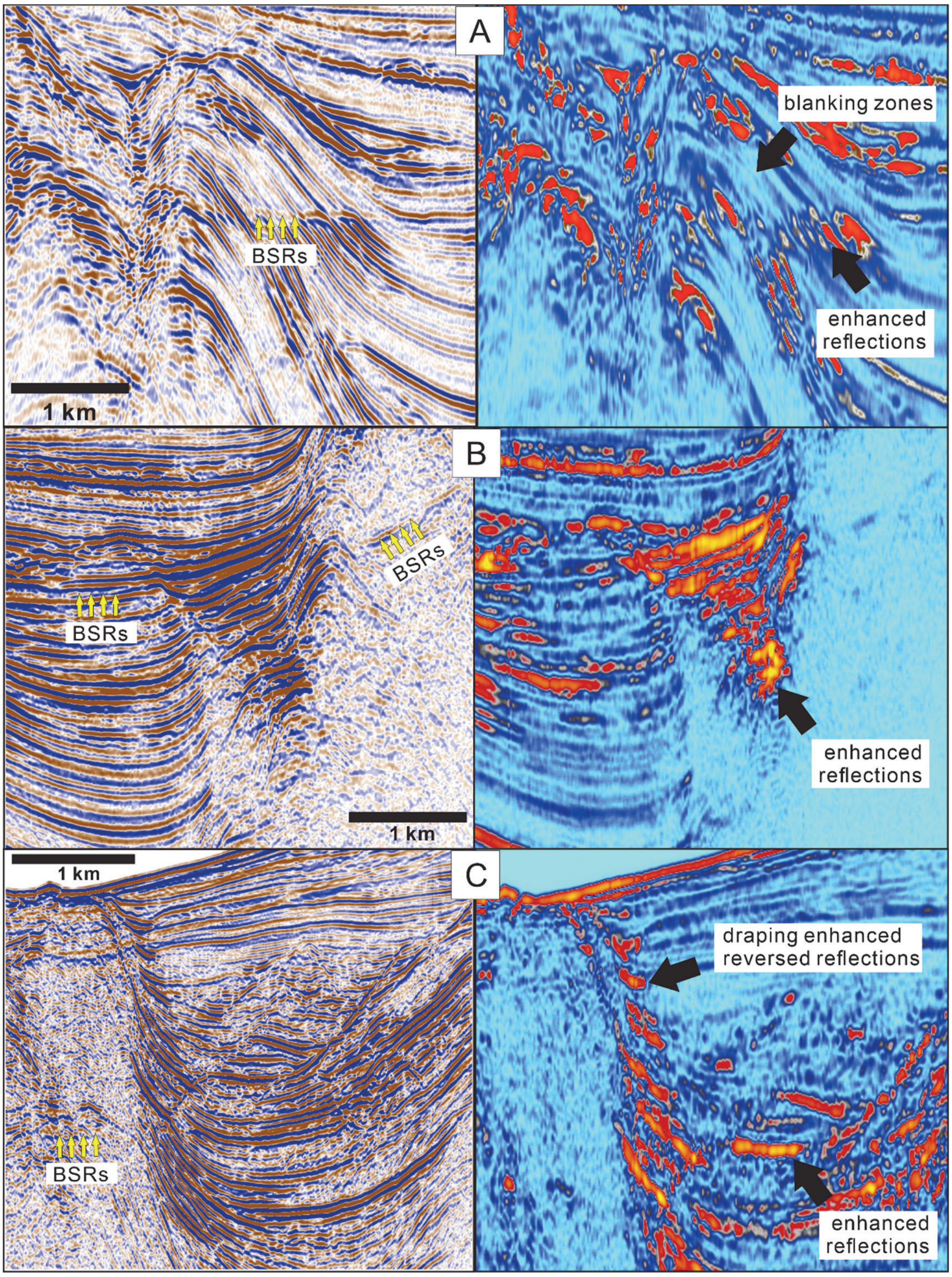


**Fig. 11. Comparison of conventional seismic and envelope attribute profiles for (A) MGL0908-TST, (B) MCS937-18, and (C) MCS937-79. Together with phase information, the attribute was used to delineate free gas and gas-hydrate bodies. Blanking zones are present above the BSRs and also commonly occur below BSRs; enhanced reversed reflections are also visible above BSRs.**

act as dewatering catalysts for previously preserved gas hydrates. The dissociated gases migrate upward and laterally, and accumulate in traps at the flanks of diapiric bodies. As a natural gas pathway, mud diapirs may contribute to the migration of deep-seated thermogenic gas into the GHSZ. The insufficient quantity of water required to recrystallize and re-encapsulate the dissociated gas promotes the existence of bright, reversed polarity reflections although being preserved within the GHSZ.

The intrusion of overpressured mud may initiate brittle fault zones in the overlying strata. Lacombe *et al.* (2004) suggested that the diapirs in offshore southwestern Taiwan developed from thrust-related anticlines, which formed when deformation propagated into the area. The thrust faults may have provided conduits for mud and fluid migration. Previous studies have shown evidence for fluid migration along fault zones and *décollements* in the Barbados (Westbrook and Smith, 1983) and Nankai accretionary wedges

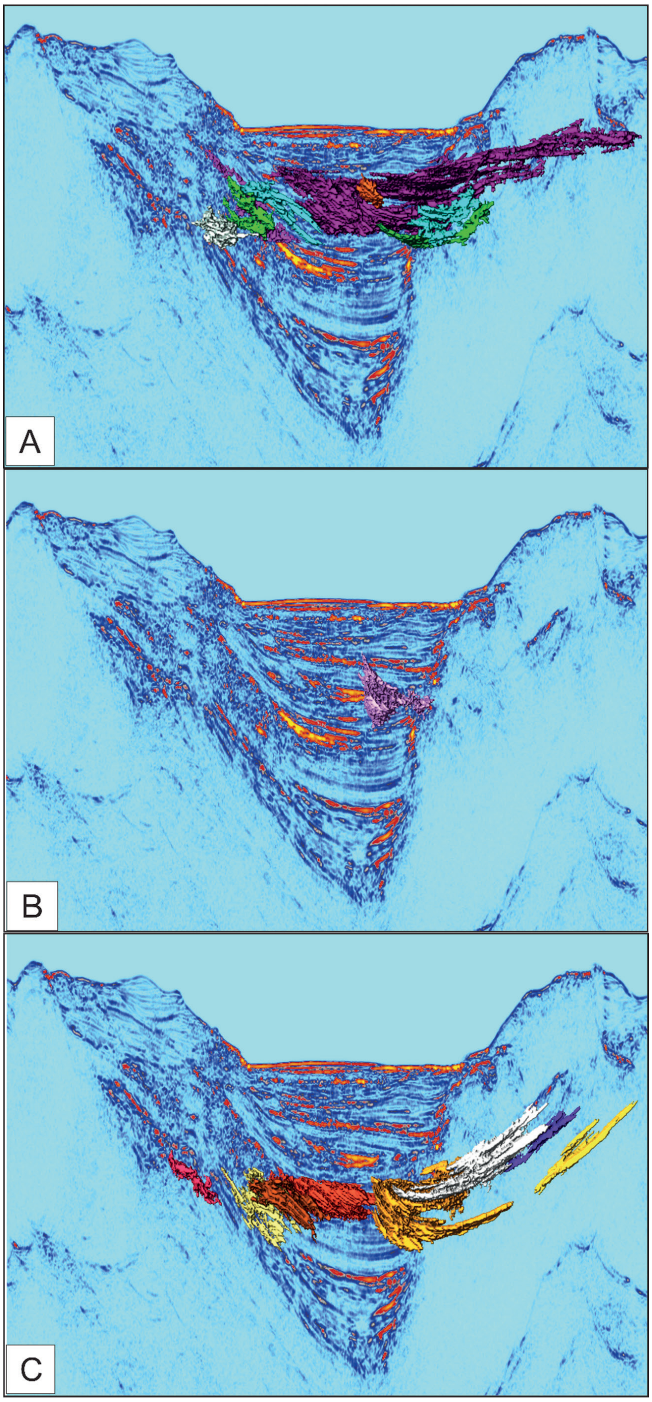


**Fig. 12. Geobody extraction based on amplitude-driven attributes for (A) gas-hydrate compartments above BSRs, (B) free gas compartments above BSRs and (C) free gas compartments below BSRs. The geobody colours represent different voxel volumes generated from amplitude opacity.**

(Moore *et al.*, 2001). These examples support a means for transporting methane over considerable distances into the GHSZ. Blanking reflections within the diapir-induced faults indicate gas-bearing fluid conduits. Strong reflections at the sides of mud diapirs (e.g. flank drags) or next to fault zones can be interpreted in terms of high gas contents, demonstrating the presence of gas fluxes (Figs 7, 8, 9). When diapirism is accompanied by excessive fluid fluxes, it drags the adjacent strata, causing it to rotate and fail at roll-over normal faults (Fig. 9). These faults may serve as a possible pathway for deeper fluids to migrate upwards. The low permeability nature of mud increases the sealing capability when free gas-charged layers are trapped against mud diapirs, and is expressed by high amplitude reflections dragging on diapiric flanks with a reversed phase relative to that of the seafloor (Fig. 10). Both growth strata and normal strata are discernable, suggesting the dynamics of mud diapiric development through time (Figs 7, 8, 9). Growth strata are developed during periods of active intrusion, whereas normal strata mark quiescent deposition during inter-intrusion periods. Previous studies (e.g. Hsu *et al.*, 2013; Hsiung *et al.*, 2014) have reported relationships between growth strata versus accumulation rates in the Gaoping slope. Should the basin subside during deposition, e.g. during mud diapiric intrusion, the reflection characteristics would be sub-parallel, and in general would converge towards the basin margin and diverge toward the axis. Overlying, more gently dipping strata, with onlapping reflections terminating against the diapirs at shallow depths indicates times when the diapirs became inactive.

Concealed at relatively shallower depths in the southern part of the study area, a buried mud diapir is present in the central part of the basin (Figs 6, 9) and may provide a feeder channel which permits fluid flow to shallower strata. Hsu *et al.* (2017) identified the buried mud diapir as a plunging fold where it connects to the northern flank of the Lower Fangliao Basin and converges with diapir ridges at the western flank. Based on geochemical analyses, You *et al.* (2004) proposed that mud volcanoes onshore Taiwan exhibit intensive dewatering from accretionary wedges through mud diapirism. Although the mud diapir is buried in deeper strata, it still permits hydrocarbons to migrate upwards, increasing the fluid saturation of overlying strata through diffusion.

In many convergent margins, hydrocarbon gas leakage is often associated with structures such as mud diapirs (Westbrook and Smith, 1983; Barber *et al.*, 1986; Satyana and Asnidar, 2009). Oversaturated fluids weaken overlying strata and may lead to collapsed domes/anticlines, forcing hydrocarbon to be trapped in shallower strata, e.g. as buried pockmarks (Fig. 7). This relief is visible on seismic data in terms of negative collapse features with high amplitude reflections. In the Gulf of Patras, Greece, similar reflection characteristics may be due to possible continual gas venting (Hasiotis *et al.*, 1996).

The gas within the study area is inferred to be either microbial (Chuang *et al.*, 2010; Chen *et al.*, 2014) or thermogenic (Sun *et al.*, 2010). This indicates that biogenic gas can be an alternative source for free gas or gas-hydrate accumulations where thermogenic gas is not available.

Due to the absence of exploration drilling, the possible source of thermogenic gas is yet to be determined. Based on seismic interpretations, it is likely that the thermogenic gas migrates into the GHSZ by means of three mechanisms: (i) focused advection along fluid escape structures (e.g. buried mud diapirs) (Fig. 7); (ii) advective migration along permeable, dipping strata (Fig. 8); and (iii) diffusion following hydrate decomposition due to the interplay of sedimentation and mud diapir intrusion (Fig. 9).

Fluid flow in the study area is characterized by low vertical fluid migration rates, approximately 6 cm/y based on regional fluid flow studies from BSRs (Chen *et al.*, 2012), consistent with the presence of thick hemipelagic sediments. Deep-seated faults may not cut through shallower strata, hence limiting upward fluid migration. Hu *et al.* (2017) suggested that relatively low methane concentrations and flux occur in the Lower Fangliao Basin (4.5 mmol. $m^{-2}.y^{-1}$) compared to neighbouring areas based on geochemical analyses of cores recovered from a few metres below the seafloor.

However, methane flux cannot be treated as an exclusive subsurface gas-hydrate indicator. Limited core length could have hindered the detection of deep gas hydrates from the geochemical measurements. An alternative suggestion has been proposed by Horng *et al.* (2016), where the presence of iron-sulphide minerals in sediments in the Lower Fangliao Basin could indirectly be influenced by the high methane supply. There is a positive relationship between the methane supply and the presence of iron sulphide minerals in sediments above methane hydrate-bearing sites in the Carolina Rise and Blake Ridge (Musgrave and Hiroki, 2000). The persistence of such minerals in sediments requires a continual supply of methane overcoming the losses due to diffusion or advection (Riedel *et al.*, 2006). These conditions can be achieved (i) if there is a sufficiently large supply of organic matter to permit shallow methanogenic decomposition, or (ii) if there is ample upward methane flux related to fault zones or other possible conduits, such as mud diapirs. Together with fault activity, vertical venting may be controlled by mud diapirs and these are the dominant methods of forming thermogenic gas seepages in the Lower Fangliao Basin.

**Volumetric evaluations**

Based on Monte Carlo simulations, the estimated volume of in-place gas in the study area is ~ 2048 Bcf (Fig. 13). Gas-hydrate prospects above BSRs potentially hold the most significant volumes (1251.05 Bcf), followed by free gas below BSRs (717.52 Bcf) and free gas above BSRs (80.18 Bcf).

This study utilized geobody extraction to derive prospect volumes and thicknesses. The method has been proposed in other studies (Larue and Hovadik, 2006; Hovadik and Larue, 2007) as an alternative to deriving the gross rock volumes in the absence of well information. Unlike conventional studies in which there is assumed to be a gas-hydrate dominated zone at depth over BSRs, this study infers the presence of free gas within the GHSZ.

Enhanced reversed polarity above BSRs (Figs 9, 10) is evidence of higher-impedance sediments overlying lower-impedance gas-filled sediments. This could occur when free gas in the reservoir saturates the available pore water volume. Intrusion of a mud diapir with a relatively high thermal conductivity may locally perturb the gas hydrate stability phase, allowing free gas to be trapped against the flanks of mud diapirs within the GHSZ.

The stability and distribution of gas hydrates and free gas are dependent on pore pressure, geothermal gradient, sediment thermal conductivity, sediment

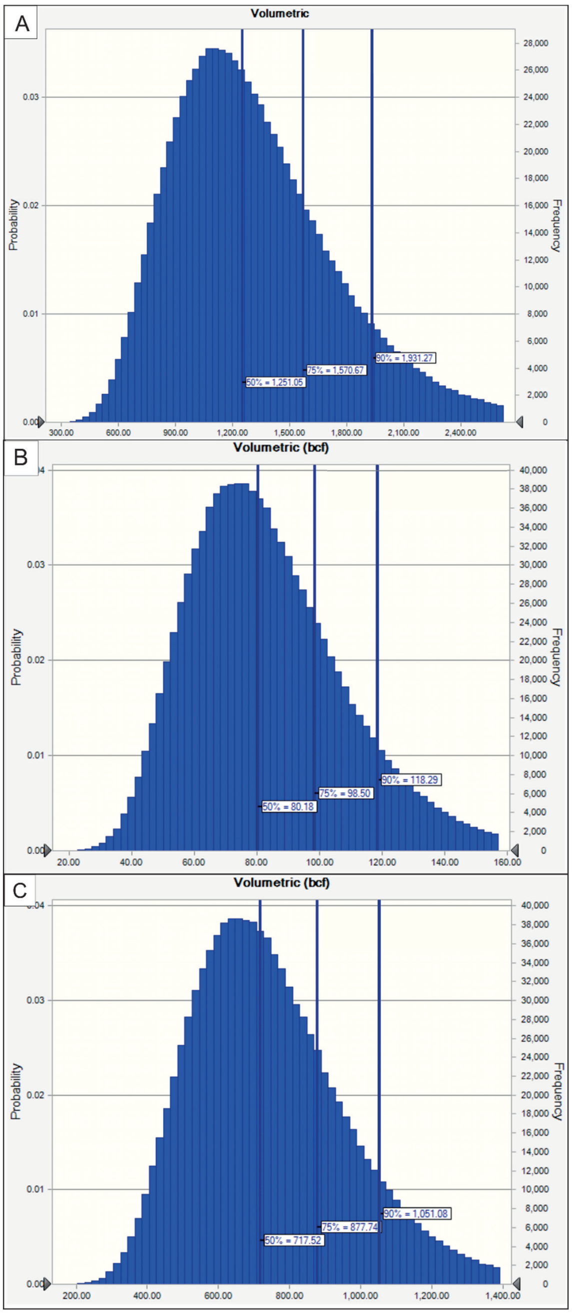


**Fig. 13. Probabilistic distribution of in-place gas volumes for (A) gas-hydrate compartments above BSRs, (B) free gas compartments above BSRs, and (C) free gas compartments below BSRs in the study area.**

grain size and mineralogy, effective stress, pore water salinity, gas solubility and pore water availability (Bahk *et al.*, 2013). Since thresholds for each reservoir parameter are related to the baseline proxies from previous studies, which may not be accurate in the absence of core samples, uncertainties in the estimates must be expected. Nevertheless, this study presents a first-order estimate of methane-bearing zones in the Lower Fangliao Basin and will contribute to future deep-sea hydrocarbon exploration in offshore southwestern Taiwan.

## CONCLUSIONS

Controls by mud diapirs on gas-hydrate and free gas preservation in the Lower Fangliao Basin, offshore southwestern Taiwan, were investigated using multichannel seismic data. The gas-hydrate and free gas zonation within the GHSZ is characterized by (i) high amplitude reflections with a phase analogous to that of seafloor, indicating possible porous turbidite sand-rich reservoirs; (ii) BSRs showing polarity reversal relative to seafloor, suggesting higher impedance, gas hydrate-charged intervals overlying lower impedance intervals with free gas; (iii) blanking reflections in the fault zones, interpreted as gas-bearing fluid conduits; (iv) strong reflections on the flanks of mud diapirs (e.g. flank drags) and above buried mud diapirs, demonstrating the presence of gas hydrates; (v) high amplitude reflections dragging on diapiric flanks with reversed phases relative to that of seafloor, indicating free-gas charged sediments abutting mud diapirs; and (vi) focused advection and diffusion flow through mud diapirs and faults, which may control thermogenic gas migration. On the basis of 3D seismic interpretations, the hydrocarbon zones can be divided into gas-hydrate compartments above BSRs, free gas compartments above BSRs, and free gas compartments below BSRs. Monte-Carlo simulations were used to determine first-order estimates of the total gas volume in the study area, which is inferred to total about 2048 Bcf. This study serves as a preliminary estimate of the natural gas potential of the upper accretionary wedge offshore southwestern Taiwan.

## ACKNOWLEDGEMENTS

We thank JPG editorial staff and the anonymous referees for their thorough reviews and comments. This study was funded by the Central Geological Survey, Ministry of Economic Affairs, under the grants 99-5226904000-04-02 and 104-5226904000-02-01.

## REFERENCES

BAHK, J.J., KIM, D.H., CHUN, J.H., SON, B.K., KIM, J.H, RYU, B.J., TORRES, M.E., RIEDEL, M. and SCHULTHEISS, P., 2013. Gas hydrate occurrences and their relation to host sediment properties: Results from second Ulleung Basin gas hydrate drilling expedition, East Sea. *Marine and Petroleum Geology*, **47**, 21–29.

BARBER, A.J., TJOKROSAPOETRO, S. and CHARLTON, T., 1986. Mud volcanoes, shale diapirs, wrench fault and melanges in accretionary complexes, eastern Indonesia. *AAPG Bull.*, **70**, 1729-1741.

BASOV, E.I., VAN WEERING, T.C.E., GAEDIKE, C., BARANO, B.V., LELIKOV, E.P., OBZHIROV, A.I. and BELYKH, I.N., 1996. Seismic facies and specific character of the bottom simulating reflector on the western margin of Paramushir Island, Sea of Okhotsk. *Geo-Marine Letters*, **16**, 297- 304.

BROOKS, J.M., COX, H.B., BRYANT, W.R., KENNICUTT, M.C., MANN, R.G. and MCDONALD, T.J., 1988. Association of gas hydrate sand oil seepage in the Gulf of Mexico. *Organic Geochemistry*, **10**, 221-234.

BROWN, L.F. and FISHER, W.L., 1982. Seismic stratigraphic interpretation and petroleum exploration. *AAPG Continuing Education Course Note Series* **16**.

CHEN, L., CHI, W.C., LIU, C.S., SHYU, C.T., WANG, Y. and LU, C.Y., 2012. Deriving regional vertical fluid migration rates offshore southwestern Taiwan using bottom-simulating reflectors. *Marine Geophysical Research*, **33** (4), 379-388.

CHEN, S.C., HSU, S.K., WANG, Y., CHUNG, S.H., CHEN, P.C., TSAI, C.H., LIU, C.S., LIN, H.S. and LEE, Y.W., 2014. Distribution and characters of the mud diapirs and mud volcanoes off southwest Taiwan. *Journal of Asian Earth Sciences*, **92**, 201-214.

CHEN, N.C., YANG, T.F., HONG, W.L., CHEN, H.W, CHEN, H.C., HU, C.Y., HUANG, Y.C., LIN, S., LIN, L.H., SU, C.C., LIAO, W.Z., SUN, C.H., WANG, P.L., YANG, T., JIANG, S.Y., LIU, C.S., WANG, Y. and CHUNG, S.H., 2017. Production, consumption, and migration of methane in accretionary prism of southwestern Taiwan. *Geochemistry, Geophysics, Geosystems*, **18**, 2970–2989.

CHENG, W.B., LIN, S.S., WANG, T.K., LEE, C.S. and LIU, C.S., 2010. Velocity structure and gas hydrate saturation estimation on active margin off SW Taiwan inferred from seismic tomography. *Marine Geophysical Research*, **31**, 77-87.

CHI, W.C., REED, D.L., LIU, C.S. and LUNDBERG, N., 1998. Distribution of the bottom-simulating reflector in the offshore Taiwan collision zone. *Terrestrial, Atmospherics, and Ocean Sciences*, **9**, 779–794.

CHI, W.C. and REED, D.L., 2008. Evolution of shallow, crustal thermal structure from subduction to collision: An example from Taiwan. *Geol. Soc. Am. Bull.*, **120**, 679-690.

CHIANG, C.S., YU, H.S., NODA, A., TUZINO, T. and SU, C.C., 2012. Avulsion of the Fangliao submarine canyon off SW Taiwan as revealed by morphological analysis and numerical simulation. *Geomorphology*, **177-178**, 26-37.

CHUANG, P.C., YANG, T.F., HONG, W.L., LIN, S., SUN, C.H., LIN, A. T., CHEN, J.C., WANG, Y. and CHUNG, S.H., 2010. Estimation of methane flux offshore SW Taiwan and the influence of tectonics on gas hydrate accumulation. *Geofluids*, **10**, 497–510.

CHUNG, S.H., LIN, A.T., LIN, C.C., LIU, C.S., CHEN, C.C., WANG, Y., WEI, C.Y. and CHEN, P.C., 2016. Geological investigation of gas hydrate resource potential in the offshore areas of south-southwest Taiwan. *Special Publications of the Central Geological Survey, Ministry of Economic Affairs*, **30**, 1-42. (in Chinese)

COLLETT, T.S., 1997. Gas hydrate resources of northern Alaska. *Bulletin of Canadian Petroleum Geology*, **45** (3), 317-338.

COLLETT, T.S., JOHNSON, A.H., KNAPP, C.C. and BOSWELL, R., 2009. Natural gashydrates - Energy resource potential and associated geologic hazard. *AAPG Memoir*, **29** (2), 858–869.

COVEY, M., 1984. Lithofacies analysis and basin reconstruction, Plio-Pleistocene western Taiwan foredeep. *Petroleum Geology of Taiwan*, **20**, 53–83.

DEFFONTAINES, B., LIU, C.S. and HSU, H.H., 2016. Structure and deformation of the Southern Taiwan accretionary prism: The active submarine Fangliao Fault Zone offshore west Hengchun Peninsula. *Tectonophysics*, **692**, 227-240.

DIRGANTARA, F., CHIANG, H.T., LIN, A.T., LIU, C.S. and CHEN, S.C., 2019 *in press*. Depositional influence of submarine channel migration on thermal properties of the Lower Fangliao Basin, offshore southwestern Taiwan. *Marine Geophysical Research, in press.*

ELLIOTT, J.R. and LIRA, C.T., 1996. An introduction to applied thermodynamics. (http://www.egr.msu.edu/~lira/thermtxt.htm, accessed on 2018/6/5).

FUJII, T., SAEKI, T., KOBAYASHI, T., INAMORI, T., HAYASHI, M., TAKANO, O., TAKAYAMA, T., KAWASAKI, T., NAGAKUBO, S., NAKAMIZU, M. and YOKOI, K., 2009. Resource assessment of methane hydrate by applying a probabilistic approach in the eastern Nankai Trough, Japan. *Journal of Geography*, **118** (5), 814-834. (in Japanese)

HAMILTON, E.L., 1980. Geoacoustic modeling of the sea-floor. *Journal of the Acoustical Society of America*, **68**, 1313-1340.

HASIOTIS, T., PAPATHEODOROU, G., KASTANOS, N. and FERENTINOS, G., 1996. A pockmark field in the Patras Gulf (Greece) and its activation during the 14/7/93 seismic event. *Marine Geology*, **130**, 333–344.

HE, W. and ZHOU, J., 2018. Structural features and formation conditions of mud diapirs in the Andaman Sea Basin. *Geological Magazine*, **156** (4), 659-668.

HOLBROOK, W.S., 2000. Seismic studies of the Blake Ridge: Implications for hydrate distribution, methane expulsion, and free gas dynamics. In: Paull, C.K. and Dillon, W.P. (Eds), Natural Gas hydrate: Occurrence, Distribution, and Detection. *Geophysical Monograph Series*, **124**, 235 – 256.

HORNG, C.S., CHEN, K.H., LIN, C.H., TSENG, C.Y., WANG, Y., FEI, L.Y, CHUNG, S.H., CHEN, S.C., CHEN, P.C., WEI, C.Y. and WANG, C.C., 2016. Rock magnetic properties of sediments in gas hydrate potential areas offshore of Southwestern Taiwan. *Special Publications of the Central Geological Survey, Ministry of Economic Affairs*, **30**, 89-122.

(in Chinese)

HOVADIK, J. and LARUE, D.K., 2007. Static characterizations of reservoirs: Refining the concepts of connectivity and continuity. *Petroleum Geoscience*, **13**, 195-211.

HSIUNG, K.H., YU, H.S. and CHIANG, C.S., 2014. Seismic characteristics, morphology and formation of the ponded Fangliao Fan off southwestern Taiwan, northern South China Sea. *Geo-Marine Letters*, **34**, 59-74.

HSU, H.H., LIU, C.S., YU, H.S., CHANG, J.H. and CHEN, S.C., 2013. Sediment dispersal and accumulation in tectonic accommodation across the Gaoping Slope, offshore Southwestern Taiwan. *Journal of Asian Earth Sciences*, **69**, 26–38.

HSU, H.H., LIU, C.S., CHANG, Y.T., CHANG, J.H., KO, C.C., CHIU, S.D. and CHEN, S.C., 2017. Diapiric activities and intraslope basin development offshore of SW Taiwan: A case study of the Lower Fangliao Basin gas hydrate prospect. *Journal of Asian Earth Sciences*, **149**, 145-159.

HSU, S.K., CHIANG, C.W., EVANS, R.L., CHEN, C.S., CHIU, S.D., MA, Y.F., CHEN, S.C., TSAI, C.H., LIN, S.S. and WANG, Y., 2014. Marine controlled source electromagnetic method used for the gas hydrate investigation in the offshore area of SW Taiwan. *Journal of Asian Earth Sciences*, **92**, 224-232.

HU, C.Y., YANG, T.F., CHUANG, P.C., CHEN, H.W., CHEN, N.C., HUANG, Y.C., LIN, S., WANG, Y., CHUNG, S.H., HUANG, C.D. and CHEN, C.H., 2017. Biogeochemical cycles at the sulfate-methane transition zone (SMTZ) and geochemical characteristics of the pore fluids offshore southwestern Taiwan. *Journal of Asian Earth Sciences*, **148**, 172-183.

HUH, C.A., LIN, H.L., LIN, S. and HUANG, Y.W., 2009. Modern accumulation rates and a budget of sediment off the Gaoping (Kaoping) River, SW Taiwan: A tidal and flood dominated depositional environment around a submarine canyon. *Journal of Marine Systems*, **76** (4), 405–416.

JOHNSON, J.E., MIENERT, J., FAVEROLA, A.P., VADAKKEPULIYAMBATTA, S., KNIES, J., BUNZ, S., ANDREASSEN, K. and FERRE, B., 2015. Abiotic methane from ultraslow-spreading ridges can charge Arctic gas hydrate. *Geology*, **43** (5), 371-374.

LACOMBE, O., ANGELIER, J., MOUTHEREAU, F., CHU, H.T., DEFFONTAINES, B., LEE, J.C., ROCHER, M., CHEN, R.F. and SIAME, L., 2004. The Liuchiu Hsu island offshore SW Taiwan: Tectonic versus diapiric anticline development and comparisons with onshore structures. *Comptes Rendus Geoscience*, **336**, 815-825.

LARUE, D.K. and HOVADIK, J., 2006. Connectivity of channelized reservoirs: A modelling approach. *Petroleum Geoscience*, **12**, 291-308.

LEE, M.W. and COLLETT, T. S., 2012. Pore- and fracture-filling gas hydrate reservoirs in the Gulf of Mexico Gas Hydrate Joint Industry Project Leg II Green Canyon 955 H well. *Marine and Petroleum Geology*, **34**, 62–71.

LEE, T.Y., TANG, C.H., TING, J.S. and HSU, Y.Y., 1993. Sequence stratigraphy of the Tainan Basin, offshore southwestern Taiwan. *Petroleum Geology of Taiwan*, **28**, 119-158.

LI, L., LEI, X., ZHANG, X. and SHA, Z., 2013. Gas hydrate and associated free gas in the Dongsha Area of northern South China Sea. *Marine and Petroleum Geology*, **39**, 92-101.

LIN, A.T. and WATTS, A.B., 2002. Origin of the West Taiwan basin by orogenic loading and flexure of a rifted continental margin. *Journal of Geophysical Research*, **107** (B9), 2185.

LIN, A.T., WATTS, A.B. and HESSELBO, S.P., 2003. Cenozoic stratigraphy and subsidence history of the South China Sea margin in the Taiwan region. *Basin Research*, **15** (4), 453-478.

LIN, A.T., LIU C.S., LIN C.C., SCHNURLE, P., CHEN G.Y., LIAO W.Z., TENG L.S., CHUANG, H.J. and WU, M.S., 2008. Tectonic features associated with the overriding of an accretionary wedge on top of a rifted continental margin: An example from Taiwan. *Marine Geology*, **255**, 186-203.

LIN, A.T., YAO, B., HSU, S.K., LIU, C.S. and HUANG, C.Y., 2009a. Tectonic features of the incipient arc-continent collision zone of Taiwan: Implications for seismicity. *Tectonophysics*, **479**, 28-42.

LIN, C.C., LIN, A.T., LIU, C.S, CHEN, G.Y., LIAO, W.Z. and SCHNURLE, P., 2009b. Geological controls on BSR occurrences in the incipient arc-continent collision zone off southwest Taiwan. *Marine and Petroleum Geology*, **26**, 1118–1131.

LIN, C.C., LIN, A.T., LIU, C.S., HORNG, C.S., CHEN, G.Y. and WANG, Y., 2014. Canyon-infilling and gas hydrate occurrences in the frontal fold of the offshore accretionary wedge off southern Taiwan. *Marine Geophysical Research*, **35**, 21-35.

LIU, C. S., SCHNURLE, P., WANG Y., CHUNG, S. H., CHEN, S. C. and HSIUAN, T. H., 2006. Distribution and characters of gas hydrate offshore of southwestern Taiwan. *Terrestrial, Atmospheric and Ocean Sciences*, **17**, 615 – 644.

MAJUMDAR, U. and COOK, A.E., 2018. The volume of gas hydrate-bound gas in the northern Gulf of Mexico. *Geochemistry, Geophysics, Geosystems*, **19** (11), 4313-4328.

MCDONNELL, S.L., MAX, M.D., CHERKIS, N.Z. and CZAMECKI, M.F., 2000. Tectono-sedimentary controls on the likelihood of gas hydrate occurrence near Taiwan. *Marine and Petroleum Geology*, **17**, 929-936.

MILKOV, A.V., 2000. Worldwide distribution of submarine mud volcanoes and associated gas hydrate. *Marine Geology*, **167**, 29-42.

MILKOV, A.V., 2005. Global distribution of mud volcanoes and their significance as an indicator of active petroleum systems, a source of methane in the atmosphere and hydrosphere, and a geohazard. In: Martinelli, G. and PANAHI, B. (Eds.): Mud Volcanism, Geodynamics and Seismicity, NATO Science Series Volume, Springer, 29-34.

MOORE, G.F., TAIRA, A., KLAUS, A., BECKER, L., BOECKEL, B., CRAGG, B.A., DEAN, A., FERGUSSON, C.L., HENRY, P., HIRANO, S., HISAMITSU, T., HUNZE, S., KASTNER, M., MALTMAN, A.J., MORGAN, J.K., MURAKAMI, Y., SAFFER, D.M., SÁNCHEZ-GÓMEZ, M., SCREATON, E.J., SMITH, D.C., SPIVACK, A.J., STEURER, J., TOBIN, H.J., UJIIE, K., UNDERWOOD, M.B. and WILSON, M., 2001. New insights into deformation and fluid flow processes in the Nankai Trough accretionary prism: Results of Ocean Drilling Program Leg 190. *Geochemistry, Geophysics, Geosystems*, **2**, GC000166.

MUSGRAVE, R. J. and HIROKI, Y., 2000. Rock magnetism of the diapirs sites (sites 991, 992, and 996), Caroline Rise and Blake Ridge. In: Paull, C. K., Matsumoto, R., Wallace, P. J. and DILLON, W. P. (Eds.): Proceedings of the Ocean Drilling Program, *ODP Final Technical Report*, **164**, 401-409.

PENG, D.Y. and ROBINSON, D.B., 1976. A new two-constant equation of state. *Industrial ad Engineering Chemistry Fundamentals*, **27**, 59-64.

REED, D. L., LUNDBERG, N., LIU, C.S. and KUO, B.Y., 1992. Structural relations along the margin of the offshore Taiwan accretionary wedge: Implications for accretion and crustal kinematics. *Acta Geologica Taiwanica*, **30**, 105-122.

RIEDEL, M., NOVOSEL, I., SPENCE, G.D., HYNDMAN, R.D., CHAPMAN, R.N., SOLEM, R.C. and LEWIS, T., 2006. Geophysical and geochemical signatures associated with gas hydrate-related venting in the northern Cascadia margin. *Geol. Soc. Am. Bull.*, **118**, 23-28.

RIEDEL, M., COLLETT, T.S., KUMAR, P., SATHE, A.V. and COOK, A., 2010. Seismic imaging of a fractured gas hydrate system in the Krishna-Godavari Basin offshore India. *Marine and Petroleum Geology*, **27**, 1476–1493.

RIEDEL, M., BAHK, J.J., KIM, H.S., SCHOLZ, N.A., YOO, D.G., KIM, W.S., RYU, B.J. and LEE, S.R, 2013. Seismic facies analyses as aid in regional gas hydrate assessments. Part II: Prediction of reservoir properties, gas hydrate petroleum system analysis, and Monte Carlo simulation. *Marine and Petroleum*

*Geology*, **27**, 269-290.

SANGREE, J.B. and WIDMIER, M., 1978. Seismic stratigraphy and global changes of sea level, part 9: Seismic interpretation of clastic depositional facies. In: Payton, C. E. (Eds): Seismic stratigraphy – applications to hydrocarbon exploration. *AAPG Memoir*, **26**, 165-184.

SATYANA, A.H. and ASNIDAR., 2009. Mud diapirs and mud volcanoes in depressions of Java to Madura: Origins, natures, and implications to petroleum system. *32nd Indonesian Petroleum Association Annual Convention Proceedings*, 139-158.

SCHNURLE, P., HSIUAN, T.H. and LIU, C.S., 1999. Constraints on free gas and gas hydrate bearing sediments from multi-channel seismic data, offshore southwestern Taiwan. *Petroleum Geology of Taiwan*, **33**, 21-42.

SCHNURLE, P., LIU, C.S., HSIUAN, T.H. and WANG, T.K., 2004. Characteristics of gas hydrate and free gas offshore southwestern Taiwan from a combined MCS/OBS data analysis. *Marine Geophysical Research*, **25**, 157–180.

SHYU, C.T., HSU, S.K. and LIU, C.S., 1998. Heat flows off southwest Taiwan: Measurements over mud diapirs and estimated from bottom simulating reflectors. *Terrestrial, Atmospherics, and Ocean Sciences*, **9**, 795-812.

SHYU, C.T., CHEN, Y.J., CHIANG, S.T. and LIU, C.S., 2006. Heat flow measurement over bottom simulating reflectors, offshore southwestern Taiwan. *Terrestrial, Atmospherics, and Ocean Sciences*, **17**, 845-869.

SLOAN, Jr., E.D., 1998. Clathrate hydrate of natural gases. Marcel Dekker, New York, 705pp.

SUN, S.C. and LIU, C.S., 1993. Mud diapirs and submarine channel deposits in offshore Kaohsiung-Hengchun, southwest Taiwan. *Petroleum Geology of Taiwan*, **28**, 1-14.

SUN, C.H., CHANG, S.C., KUO, C.L., WU, J.W., SHAO, P.H. and OUNG, J.N., 2010. Origin of Taiwan's mud volcanoes: Evidence from geochemistry. *Journal of Asian Earth Science*, **36**, 105-116.

SOLOVIEV, V.A. and GINSBURG, G.D., 1994. Formation of submarine gas hydrate. *Bulletin of the Geological Society of Denmark*, **41**, 86-94.

TANER, M.T., SCHUELKE, J.S., O'DOHERTY, R. and BAYSAL, E., 1994. Seismic attributes revisited. *SEG Technical Program Expanded Abstracts*, 1104-1106.

TISSOT, B.P. and WELTE, D.H., 1984. Petroleum formation and occurrence. Springer-Verlag, New York.

WESTBROOK, G.K. and SMITH, M.J., 1983. Long decollements and mud volcanoes: Evidence from the Barbados Ridge Complex for the role of high pore-fluid pressure in the development of an accretionary complex. *Geology*, **11**, 279-283.

WU, S., WANG, X., WONG, H.K. and ZHANG, G., 2007. Low-amplitude BSRs and gas hydrate concentration on the northern margin of the South China Sea. *Marine Geophysical Research*, **29** (2), 127-138.

YAMAMOTO, K., NAKATSUKA, Y., SATO, R., KVALSTAD, T.J., QIU, K. and BIRCHWOOD, R., 2015. Geohazard risk evaluation and related data acquisition and sampling program for the methane hydrate offshore production test. *Frontiers in Offshore Geotechnics*, **III**, 173.

YANG, T.F., YEH, G.H., CHUANG, P.C., HONG, W.L. and LIN, S., 2011. Offshore gas hydrates genetically related to on-land mud volcanoes in SW Taiwan: Evidences of fluid geochemistry. In: AAPG Hedberg Conference, China.

YOU, C.F., GIESKES, J.M., LEE, T., YUI, T.F. and CHEN, H.W., 2004. Geochemistry of mud volcano fluids in the Taiwan accretionary prism. *Applied Geochemistry*, **19**, 695-707.

YU, H.S. and LU, J.C., 1995. Development of the shale diapir-controlled Fangliao Canyon on the continental slope off southwestern Taiwan. *Journal of Southeast Asian Earth Sciences*, **11** (4), 265-276.

YU, H.S., 2004. An under-filled foreland basin in the northern South China Sea off southwest Taiwan: Incipient collision and foreland sedimentation. *Geophysics Monogram Series*, **149**, 159–173.

YU, S.W., TSAI, L.L., TALLING, P.J., LIN, A.T., MII, H.S., CHUNG, S.H., and HORNG, C.S., 2017. Sea level and climatic controls on turbidite occurrence for the past 26 kyr on the flank of the Gaoping Canyon off SW Taiwan. *Marine Geology*, **392**, 140-150.

ZHOU, D. and YAO, B., 2009. Tectonics and sedimentary basins of South China Sea: Challenges and Progress. *Journal of Earth Science*, **20** (1), 1-12.